Electronic Supplementary Information for

Efficient Electron Transporting and Panchromatic Absorbing FRET Cassettes Based on Aza-BODIPY and Perylenediimide Towards Multiple Metal FRET-Off Sensing and Ratiometric Temperature Sensing

Kavita Rani[a], Upendra K. Pandey[b] and Sanchita Sengupta[a]*

[a]Department of Chemical Sciences, Indian Institute of Science Education and Research (IISER) Mohali, Punjab-140306, India.

[b]Department of Electrical Engineering, School of Engineering, Shiv Nadar University, Gautam Buddha Nagar, Uttar Pradesh 201314, India.

*Email: sanchita@iisermohali.ac.in

Table of content

1. Materials and methods S2
2. Synthesis S5
3. NMR Spectra S14
4. Photophysical Properties S23
5. Electrochemical Properties S28
6. Charge carrier mobilities and Powder X-ray Diffraction S29
7. Metal ion sensing S30
8. Determination of binding constants (K_a) for aza-BODIPY S31
9. Determination of binding constants (K_a) for triads **1** and **2** S33
10. Thermodynamics of electron transfer upon metal addition in aza-BODIPY and triads S37
11. Spectroelectrochemistry S40
12. Control experiment with TEMPO S42
13. DFT calculations S43
14. References S59

1. Materials and methods

All chemicals and solvents were purchased from commercial suppliers and used without further purification. Dichloromethane (DCM) was dried over calcium hydride and distilled prior to use. Tetrahydrofuran (THF) was dried over sodium/benzophenone and distilled prior to use. Silica gel of mesh size 60-120 was used for column chromatography.

The ^{1}H and ^{13}C NMR spectra were recorded on Bruker Biospin Avance III FT-NMR400 MHz and AvanceNeo (Bruker) 500 MHz spectrometer at room temperature. Tetramethyl silane was used as internal standard.

The high-resolution mass spectra were recorded with Waters QTOF mass spectrometer. Software used for acquiring mass spectra was Flex Control, Bruker (USA) and software used for analyzing mass spectra was Flex Analysis 3.1.

UV-Vis and near-NIR spectral measurements were carried out with Carey 5000 UV/Vis spectrophotometer using a quartz cuvette with 1 cm path length. The steady state emission and excitation studies were carried out with Hitachi F7000 fluorescence spectrophotometer equipped with R928F photomultiplier expandable up to 900 nm.

The electrochemical measurements were recorded using CHI-610 electrochemical workstation from CH Instruments (USA), with a conventional three electrode single-compartment cell consisting of a glassy carbon as the working electrode, Ag/AgCl containing 1M KCl solution as the reference electrode, wire as the counter electrode and ferrocene was used for internal calibration. Cyclic voltammetry measurements were performed at a scan-rate of 50mV/s. Tetrabutylammonium hexafluorophosphate (TBAHFP) (Alfa Aesar) (0.1 M) dissolved in pre-dried DCM was used as supporting electrolyte. The solutions were purged with nitrogen prior to measurement. The electrochemical potential was internally calibrated against the standard ferrocene/ferrocenium (Fc/Fc^{+}) redox couple prior to each measurement. For calculation of thermodynamic parameters of electron transfer for compounds in presence of metal ions, CV measurements were performed with compounds in pre-dried THF in presence of TBAHFP and addition of metal ions (Co^{2+} and Fe^{3+}).

Temperature dependent fluorescence of samples were measured using temperature controlled cuvette holder for Hitachi F7000 spectrophotometer (Luma 40) from Quantum Northwest. The Luma 40 was used in the temperature range of 20 $^{\circ}$C to 60°C. Time resolved fluorescence spectra were measured by using time correlated single photon counting (TCSPC) model from Fluorocube, Horiba Jobin Yvon, NJ equipped with picosecond laser diodes as excitation source. The 510 nm and 590 nm lasers were

used as a light source for the excitation of samples and the instrument response function (IRF) was collected using Ludox (colloidal silica) solution. The width (FWHM) of IRF was ~ 250 ps and the optical pulse durations from < 70 ps were used. Highly integrated picosecond PMT modules as well as micro channel plate PMTs were used for the time resolution.

Spectroelectrochemical measurements were performed using a cell assembly (SEC-C) supplied by BAS Inc (Japan) and the assembly comprised of a Pt counter electrode, a Pt gauze working electrode, and an Ag/AgCl reference electrode in a 1.0 mm path length quartz cell. The absorption spectra were measured using an ocean optics set up connected in absorbance mode and using FLAME spectrometer. Voltages were swept in the range of -1.7 V to +1.7 V, dry DCM was used as solvent and TBAHFP was used as the supporting electrolyte. The solutions were purged with nitrogen for 10 min prior to the Spectro electrochemical measurements.

Quantum chemical density functional theory (DFT) calculations were performed on the triads **1** and **2** in ground state using Gaussian 09 program suite.[S1] The side chains in all molecules were replaced with methyl groups in order to account for the electron donating effect of the alkyl chain and at the same time reducing the computational time and cost. The studied molecules were optimized using global hybrid B3LYP functional and 6–31G (d, p) basis set in gas phase. The frontier molecular orbitals (FMO) electronic levels and FMO distribution were obtained from geometry optimization of the neutral ground state geometries.

X-ray diffraction (XRD) was carried out by spin coating samples on quartz substrates using Cu-Kα (λ = 1.5418 Å) radiation from Xeuss (Model C HP100 fm) X-ray diffractometer from Xenocs equipped with GeniX 3D source operating at 50 kV and 0.6 mA in conjunction with a multilayer mirror and Pilatus 200 hybrid pixel detector from Dectris.

Space Charge Limited Current measurements: SCLC devices with thin films

For electron mobility measurement of triads **1** and **2,** the electron-only devices (ITO/ZnO/triad **1** or triad **2**/Ag)were fabricated. ITO/ZnO and Ag electrodes were chosen as electron injecting electrodes (Ohmic) based on their work function alignment with the LUMO of triad **1** and **2.** In SCLC technique current -voltage curve characteristic of SCLC devices with thiun films of triads **1** and **2** were recorded. In SCLC technique in current voltage charecteristics a linear increase of the current is expected at lower applied voltagses (slope of 1; measured current is mainly dominated by intrisic charge carriers of the material) however at higher applied volatages a quadratic increse in the current with applied voltage (slope of 2) is observed which is mainly due to the space charge field of injected

carrier. Considering the material to be trap free, the mobility can then be extracted from the Mott-Gurney law given by equation 1[S2]:

$$J = \frac{9}{8}\varepsilon_r\varepsilon_0\mu\frac{V^2}{d^3} \qquad (1)$$

where ε_r is the relative dielectric constant of the material (2.76 for Triad **1**&**2**) and ε_0 is the permittivity of free space., *J* is the current per unit area (6.6 mm^2), V is the applied voltage and d is the thickness of the active layer of triads **1** and **2**. In case shallow traps (related to thermal energy) are present in the material, a higher order dependence of voltage (slope more than 2) is observed , however the data can still be modelled using Mott Gurney equation given by equation 1, however a field dependent charge mobility correction is introduced. In this case the mobility can be extracted using modified Mott Gurney equation 2 as follows:

$$J = \frac{9}{8}\varepsilon_r\varepsilon_0\mu\frac{V^2}{d^3}exp(0.891\gamma\sqrt{\frac{V}{d}}) \qquad (2)$$

where γ is the fitting parameter, expressing the strength of the field dependence of the mobility. For all the samples of triads **1** and **2** modified Mott Gurney equation (2) was used to extract the mobility values by fitting the measured *J*-*V* curve.

Pre-patterned indium tin oxide (ITO) (Xinyan Technologies, Taiwan, 15Ω/cm^2) were first cleaned sequentially using 5 % soap solution (Hellmanex™ III, Sigma Aldrich), distilled water, acetone and isopropyl alcohol (IPA) in an ultrasonicator. Cleaned substrates were then dried using gentle blow of nitrogen gas followed by 20 min of UV ozone (Nova Scan PSD- Pro Series) treatment at 50 °C was further carried out to remove residual residues. Zinc oxide (ZnO) sol gel solution was then spin coated at 4500 rpm for 60 sec fetching a thickness of around 28 nm. ZnO coated substrates were then annealed at 180 °C for 1 hr at ambient condition. A 10 mg/ml solution of triads **1** and triad **2** in anhydrous chloroform was then spin coated at ZnO coated substrates at 1000 rpm for 60 sec fetching a thickness of ~ 90 nm. Thickness of all the layers were measured using Dektak surface profiler. Space charge limited current (SCLC) devices were then completed by evaporating 120 nm of Ag at 1×10^{-6} mbar pressure using thermal evaporator. The active area of the fabricated devices was 6.6 mm^2. Current voltage (*J*-*V*) characteristics were performed immediately on the completed sample using Keithley 2436 B dual channel source meter. Dielectric constant of triads **1** and **2** derivatives was extracted from capacitance-voltage characteristics (ϵ_r ~ 2.76) using high-frequency LCR meter ZM2376 (NF Corporation) with an applied oscillation level voltage of 1V and frequency sweep from 20 Hz to 2 MHz.

2. **Synthesis**

Synthesis for Perylene diimide (PDI) energy donor subchromophore

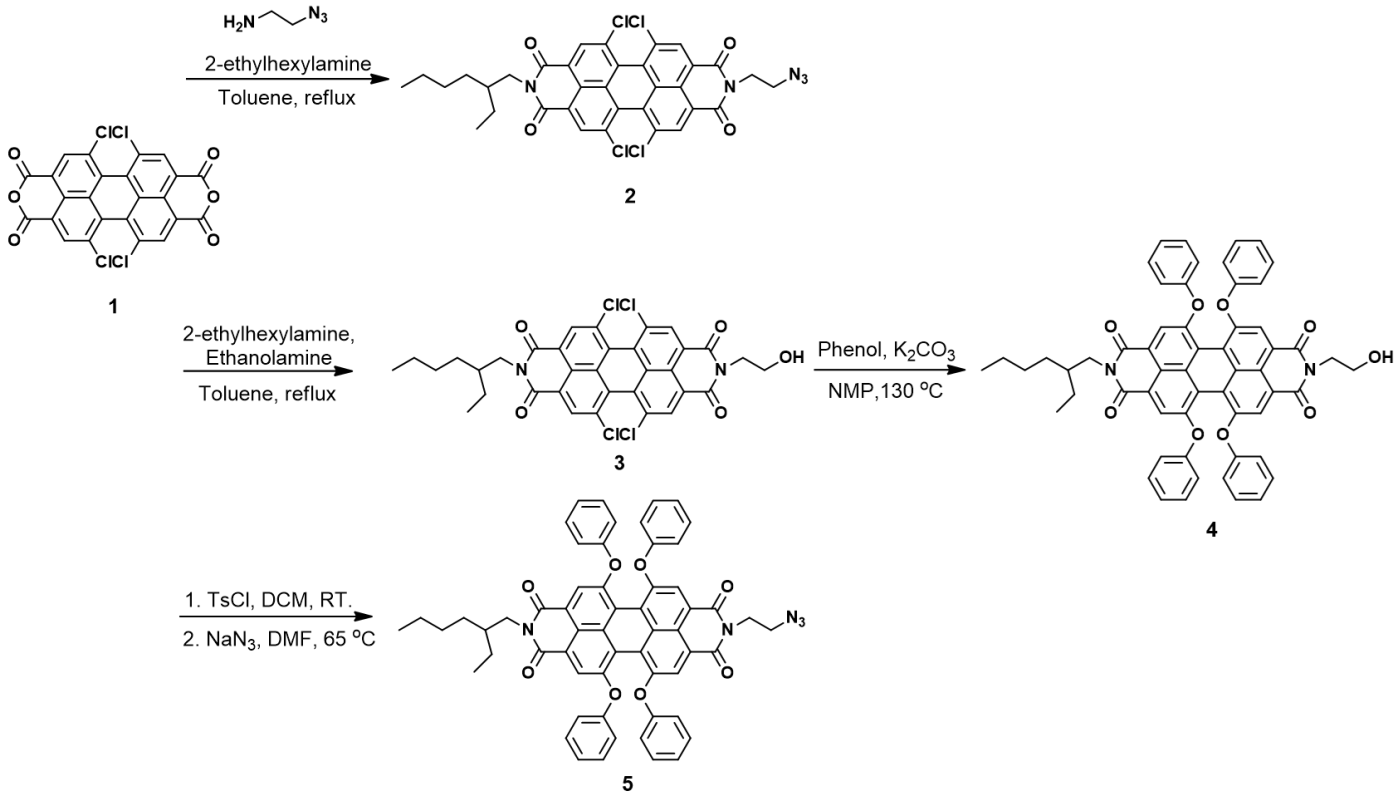

Scheme S1. Synthesis of energy donor subchromophores PDI **2** and PDI **5**.

Synthesis of compound 1

Perylene-3,4,9,10-tetracarboxylic bisanhydride (1 g, 2.55 mmol) and iodine (170 mg, 0.67 mmol) were dissolved in chlorosulfonic acid (10 mL). The mixture was heated at 70 °C for 5 h. After being cooled to room temperature (RT), mixture was poured into ice and the insoluble product was collected by filtration and washed with water. The crude product **1** (Scheme S1) was dried under vacuum and used without further purification.[S3]

Yield: 1.1 g (81 %).

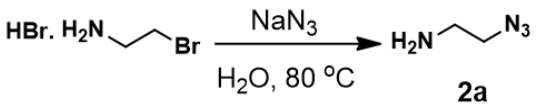

Scheme S2. Synthesis of 2-azido ethanamine (**2a**).

Synthesis of 2-azidoethanamine (2a)

Sodium azide (3.14 g, 48.30 mmol) was dissolved in 50 mL of water and to this solution, 2-bromoethylaminehydrobromide (2 g, 16.13 mmol) was added and mixture was heated at 80 °C for 24

h. After that mixture was cooled to RT, potassium hydroxide (KOH) (0.9 g, 16.04 mmol) was added to this reaction mixture at 0°C. The product was extracted with diethyl ether and washed with water, organic layer was dried over sodium sulphate and solvent was removed under reduced pressure. The product was obtained as colorless oil and used for further reaction without storage.[S4]

Yield: 678 mg (81 %).

Synthesis of compound 2

Compound **1** (500 mg, 0.94 mmol) was dissolved in dry toluene, 2-ethylhexylamine (0.15 mL, 0.94 mmol) was added and mixture was stirred for 10 minutes under nitrogen atmosphere, subsequently compound **2a** (162 mg, 1.88 mmol) was added and stirred for 10 minutes at room temperature and then refluxed for 24 h. Then solvent was removed under reduced pressure and the compound was purified by column chromatography with DCM/hexane (2/1) as eluent to obtain **2** as red solid.

Yield: 200 mg (30%).

^{1}H NMR (500 MHz, $CDCl_3$) δ (ppm): 8.71 (s, 2 H), 8.68 (s, 2 H), 4.48 (t, J = 5 Hz, 2 H), 4.20 - 4.11 (m, 2 H), 3.70 (t, J = 5 Hz, 2 H), 1.95 - 1.93 (m, 1 H), 1.42 - 1.38 (m, 4 H), 1.35-1.30 (m, 4 H), 0.97-0.93 (m, 3 H), 0.91 - 0.88 (m, 3 H).

^{13}C NMR (125 MHz, $CDCl_3$) δ (ppm): 162.71, 162.47, 135.69, 135.48, 133.37, 133.16, 131.61, 131.54, 129.11, 128.56, 123.51, 123.48, 123.42, 122.85, 48.91, 44.75, 39.39, 38.11, 30.81, 28.78, 28.76, 24.12, 24.09, 23.21, 23.20, 14.27, 10.73, 10.71.

HRMS (ESI): *m/z* calcd for $C_{34}H_{25}Cl_4N_5O_4$ $(M)^+$: 707.0661, Found: 707.0867.

Synthesis of compound 3

Compound **1** (2 g, 3.22 mmol), 2-ethylhexylamine (416 mg, 3.22 mmol) and ethanolamine (196 mg, 3.22 mmol) were dissolved in dry toluene (40 mL) under nitrogen atmosphere and reaction mixture was refluxed for 24 h. After being cooled to room temperature, solvent was removed under reduced pressure and crude compound was purified by column chromatography first with DCM then with DCM/ethyl acetate (EA) (9/1) to obtain **3** as red solid.[S5]

Yield: 800 mg (31 %).

^{1}H NMR (500 MHz, $CDCl_3$) δ (ppm): 8.69 (s, 2 H), 8.68 (s, 2 H), 4.49 (t, *J* = 5 Hz, 2 H), 4.20-4.11 (m, 2 H), 4.01 (t, *J* = 5 Hz, 2 H), 1.97 - 1.92 (m, 1 H), 1.42 - 1.38 (m, 4 H), 1.35 - 1.30 (m, 4 H), 0.97 - 0.93 (m, 3 H), 0.92 - 0.88 (m, 3 H).

^{13}C NMR (125 MHz, $CDCl_3$) δ (ppm): 163.15, 162.72, 135.65, 135.45, 133.31, 133.15, 131.56, 131.51, 129.03, 128.58, 123.48, 123.44, 123.41, 123.01, 61.31, 44.75, 43.09, 38.10, 30.80, 28.77, 28.75, 24.11, 24.09, 23.20, 14.27, 14.26, 10.73, 10.71.

HRMS (ESI): *m/z* calcd for $C_{34}H_{26}Cl_4N_2O_5$ $(M)^+$:682.0596; Found: 682.0578.

Synthesis of compound 4

Compound **3** (345 mg, 0.50 mmol), phenol (522 mg, 5.54 mmol) and K_2CO_3 (766 mg, 5.54 mmol) were dissolved in dry N-methyl-2-pyrrolidone (NMP) under nitrogen atmosphere. The reaction mixture was stirred for 24 h at 130 $^\circ$C. After being cooled to room temperature, 2 M HCl was added and precipitate was formed, it was filtered and washed with water/methanol mixture. Subsequently, the crude product was purified by column chromatography with DCM/ EA (9/1) as eluent to obtain **4** as purple solid.

Yield: 200 mg (43%).

^{1}H NMR (500 MHz, $CDCl_3$) δ (ppm): 8.19 (d, *J* = 5Hz, 4 H), 7.28-7.27 (m, 2 H), 7.27-7.26 (m, 4 H), 7.25-7.24 (m, 2 H), 7.11 (t, *J* = 5 Hz, 4 H), 6.94 (d, *J* =10 Hz, 8 H), 4.39 (t, *J* = 5 Hz, 2 H), 4.08-3.98 (m, 2 H), 3.91 (t, *J* = 5 Hz, 2 H), 1.87-1.82 (m, 1 H), 1.34 - 1.30 (m, 4 H), 1.28-1.25 (m, 4 H), 0.89 - 0.84 (m, 6 H).

^{13}C NMR (125 MHz, $CDCl_3$) δ (ppm): 164.27, 163.78, 156.22, 155.90, 155.46, 155.33, 133.01, 132.88, 130.14, 124.80, 124.77, 122.95, 122.33, 121.10, 120.43, 120.36, 120.19, 120.09, 119.81, 119.68, 61.82, 44.50, 43.01, 38.19, 30.92, 28.89, 24.19, 23.18, 14.23, 10.74.

HRMS (ESI): *m/z* calcd for $C_{58}H_{47}N_2O_9^+(M+H)^+$: 915.3276; Found: 915.3250.

Synthesis of compound 5

Compound **4** (100 mg, 0.11 mmol) was dissolved in dry DCM (20 mL) and 4-dimethyl amino pyridine (1.34 mg, 0.01 mmol) was added to this solution. After cooling this mixture to 0 $^\circ$C, p-toluene sulfonyl chloride (63 mg, 0.33 mmol) and triethyl amine (0.09 mL, 0.67mmol) were added under nitrogen atmosphere. The mixture was stirred for 24 h at room temperature under nitrogen atmosphere. After the completion of reaction, mixture was diluted with DCM, washed with aqueous

sodium bicarbonate ($NaHCO_3$) and saturated brine solution. The organic layer was dried over sodium sulphate (Na_2SO_4) and solvent was removed under reduced pressure. The crude product was dissolved in dry dimethyl formamide (DMF) (20 mL) and sodium azide (14 mg, 0.2 mmol) was added under nitrogen atmosphere, mixture was stirred at 65 °C overnight. After being cooled to room temperature, reaction mixture was extracted with DCM and dried over Na_2SO_4, purified by column chromatography with hexane/DCM (1/3) as eluent and compound **5** was obtained as a purple solid.[S6]

Yield: 63 mg (62 %).

^{1}H NMR (500 MHz,$CDCl_3$) δ (ppm): 8.20 (d, J = 10 Hz, 4 H), 7.29 - 7.27 (m, 2 H), 7.27 - 7.26 (m, 4 H), 7.26 - 7.25 (m, 2 H), 7.11 (t, J = 10 Hz, 4 H), 6.94 (d, J = 10 Hz, 8 H), 4.37 (t, J = 5 Hz, 2 H), 4.09 - 3.98 (m, 2 H), 3.61 (t, J = 5.0 Hz, 2 H), 1.87 - 1.82 (m, 1 H), 1.35 - 1.23 (m, 8 H), 0.90 - 0.84 (m, 6 H).

^{13}C NMR (125 MHz, $CDCl_3$) δ (ppm): 163.78, 163.44, 156.21, 155.92, 155.41, 155.34, 133.05, 132.93, 130.15, 124.80, 122.96, 122.23, 121.07, 120.38, 120.36, 120.20, 120.13, 120.06, 119.84, 119.69, 48.97, 44.50, 39.10, 38.20, 30.93, 28.90, 24.20, 23.19, 14.23, 10.74.

HRMS (ESI): *m/z* calcd for $C_{58}H_{46}N_5O_8^+(M+H)^+$: 940.3341; Found: 940.3340.

Synthesis of Aza BODIPY energy acceptor precursor

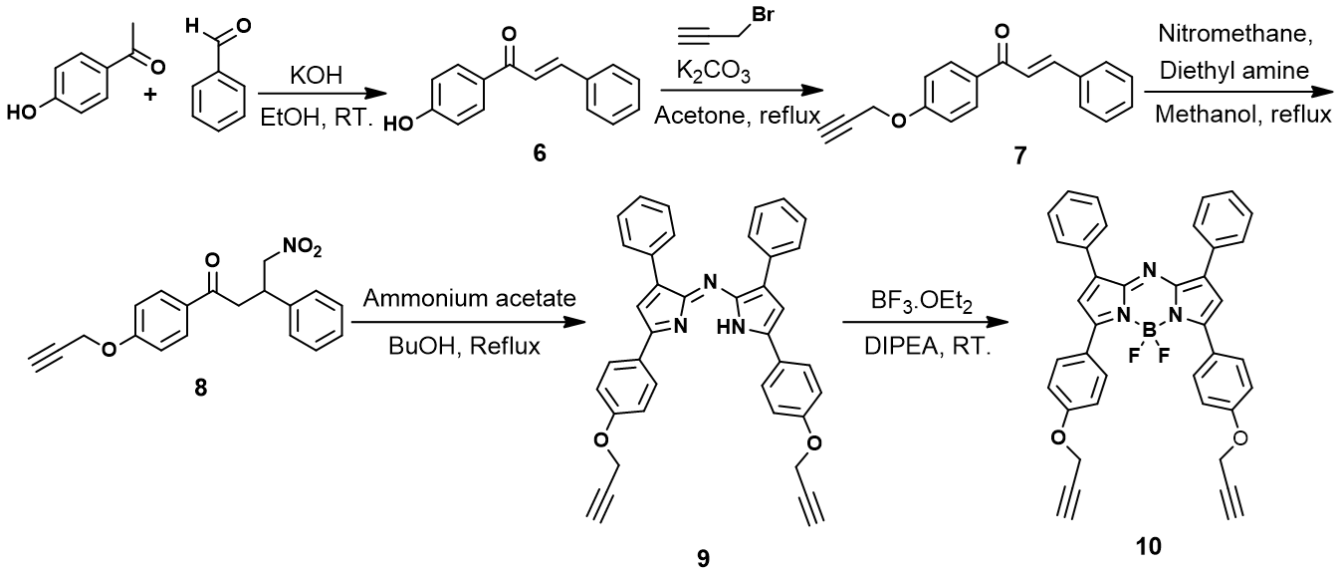

Scheme S3. Synthesis of Aza-BODIPY energy acceptor precursor **10**.

Synthesis of compound 6

4-hydroxy acetophenone (2 g, 14.68 mmol) and benzaldehyde (1.55 g, 14.68 mmol) were dissolved in EtOH (10 mL) and aqueous solution of KOH (2.47 g, 44.02 mmol) was added to this mixture dropwise at 0 °C and mixture was stirred at room temperature for 12 h. After being cooled to 0 °C, 1 M HCl was added, precipitate was formed which was filtered and washed with water and compound **6** was obtained as a pale yellow solid.

Yield: 2.8 g (85 %).

^{1}H NMR (400 MHz, MeOD) δ (ppm): 8.03 (d, J = 8 Hz, 2 H), 7.76 (s, 2 H), 7.73 (s, 2 H), 7.43 (m, 3 H), 6.91 (d, J = 8 Hz, 2 H).

Synthesis of compound 7

Compound **6** (2.5 g, 11.14 mmol) was dissolved in acetone (40 mL) followed by addition of a mixture of propargyl bromide (1.98 g, 16.71 mmol) and potassium carbonate (2.31 g, 16.72 mmol). Subsequently, the reaction mixture was refluxed for 5 h. After being cooled to room temperature, reaction mixture was filtered followed by removing the solvent of the filterate, crude product was obtained which was purified by recrystallization from methanol and a white solid compound (**7**) was obtained.[S7]

Yield: 2.65 g (91 %).

^{1}H NMR (500 MHz, $CDCl_3$) δ (ppm): 8.07 - 8.04 (m, 2 H), 7.81 (d, J = 15 Hz, 1 H), 7.65 (m, 2 H), 7.56 (d, J = 15 Hz, 1 H), 7.43 - 7.41 (m, 3 H), 7.09 - 7.06 (m, 2 H), 4.79 (d, J = 4 Hz, 2 H), 2.56 (t, J = 4 Hz, 1 H).

Synthesis of compound 8

Diethylamine (3.28 mL, 31.72 mmol) and nitromethane (1.69 mL, 31.56 mmol) were added to the solution of compound **7** (1.66 g, 6.34 mmol) in methanol (50 mL). The mixture was refluxed for 24 h. After being cooled to 0 °C, the solution was quenched with HCl (50 mL, 2.5 M). The reaction mixture was filtered and the crude product was recrystallized in methanol and white solid compound (**8**) was obtained.[S8]

Yield: 1.87 g (91 %).

^{1}H NMR (400 MHz, $CDCl_3$) δ (ppm): 7.92 (d, J = 8 Hz, 2 H), 7.35 - 7.24 (m, 5 H), 7.01 (d, J = 8 Hz, 2 H), 4.86 - 4.66 (m, 4 H), 4.25 - 4.18 (m, 1 H), 3.49 - 3.31 (m, 2 H), 2.55 (t, J = 4 Hz, 1 H).

Synthesis of compound 10

Compound **8** (1.08 g, 3.34 mmol) and ammonium acetate (9.41 g, 122.20 mmol) were dissolved in 30 mL of anhydrous butanol. The reaction mixture was refluxed for 24 h. After being cooled to RT, the precipitate was filtered and washed with cold ethanol (EtOH) to give blue solid compound **9**. This compound was used for the next step without further purification.

Yield: 425 mg (23 %)

Compound **9** (100 mg, 0.18 mmol) was dissolved in dry DCM (20 mL), then diisopropyl ethyl amine (DIPEA) (0.39 mL, 2.15 mmol) was added and mixture was stirred for 15 min at room temperature. Subsequently, $BF_3.Et_2O$ (0.39 mL, 3.20 mmol) was added dropwise and mixture was stirred at room temperature for 24 h under nitrogen atmosphere. Subsequently, the reaction mixture was washed with a saturated aqueous ammonium chloride (NH_4Cl) solution, saturated brine solution and water. The organic layer was dried over $Na_2SO_4$and the solvent was evaporated under reduced pressure. The crude product was purified by column chromatography with DCM/hexane (1/1) as eluent and to obtain green solid compound **10**.[S8]

Yield: 90 mg (83 %)

^{1}H NMR (500 MHz, $CDCl_3$) δ (ppm): 8.11 - 8.05 (m, 8 H), 7.48 - 7.40 (m, 6 H), 7.11 - 7.04 (m, 6 H), 4.77 (d, J = 2 Hz, 4 H), 2.57 (t, J = 2 Hz, 2 H).

^{13}C NMR (125 MHz, $CDCl_3$) δ (ppm): 159.97, 158.28, 145.54, 143.54, 132.56, 131.71, 129.44, 128.72, 125.08, 118.86, 115.19, 78.17, 76.22, 56.02.

HRMS (ESI): *m/z* calcd for $C_{38}H_{27}BF_2N_3O_2^+$ $(M+H)^+$: 606.2159; Found: 606.2170.

Synthesis of triad 1

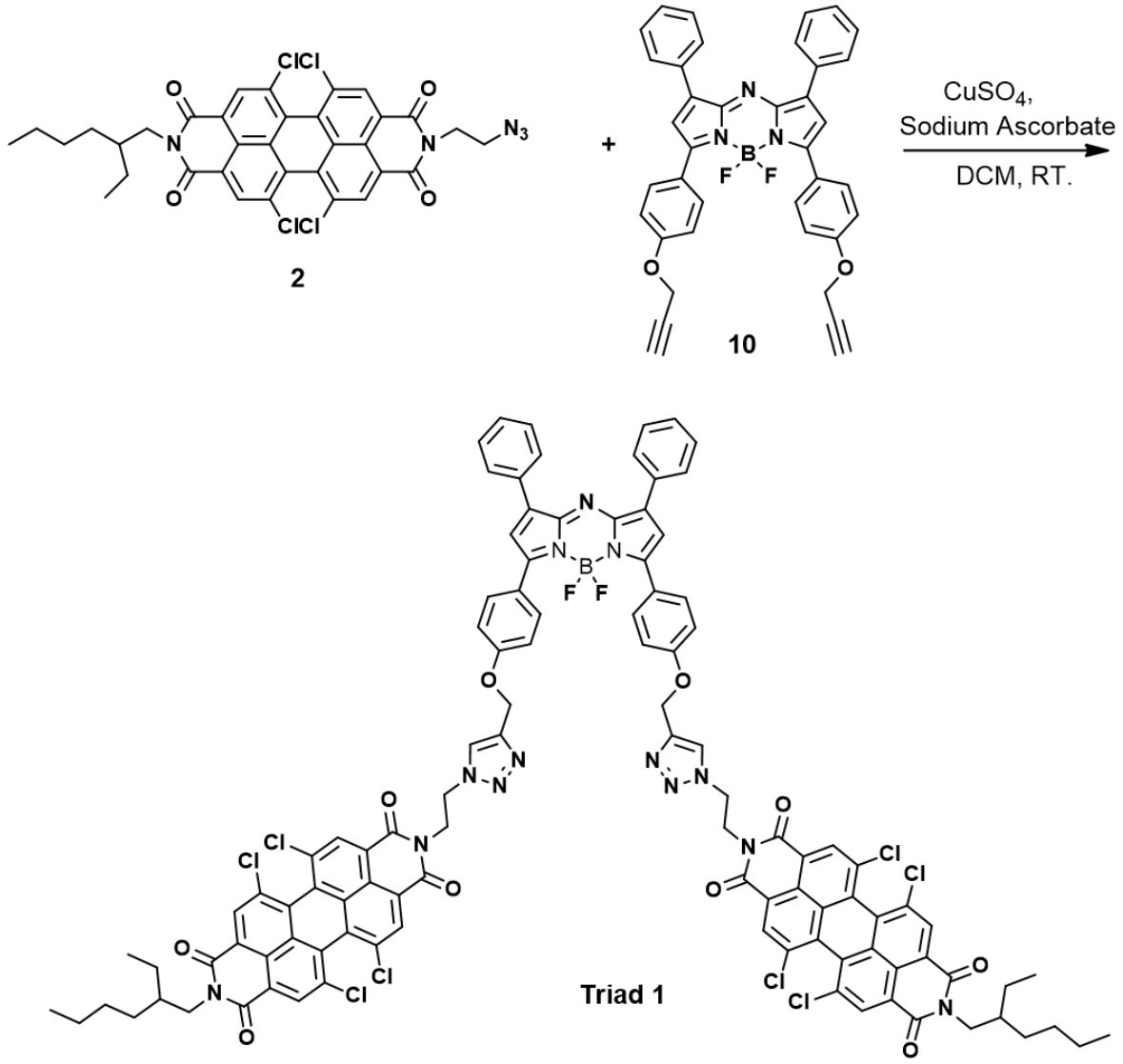

Scheme S4. Synthesis of triad **1**.

PDI compound **2** (42 mg, 0.06 mmol) was dissolved in a mixture of DCM, EtOH and water (12:1:1) under nitrogen atmosphere followed by addition of sodium ascorbate (4.42 mg, 0.02 mmol) and copper sulphate (2.85 mg, 0.01 mmol) into this mixture. After purging the reaction mixture with nitrogen for 15 minutes, compound **10** (14 mg, 0.02 mmol) was added and the reaction mixture was stirred for 24 h at room temperature. After the completion of reaction, the reaction mixture was extracted with DCM and the organic layer was dried over sodium sulphate, solvent was removed under reduced pressure. The crude product was purified by column chromatography DCM/EA (4/1) as eluent and a brown solid compound (triad **1**) was obtained.

Yield: 36 mg (78 %).

^{1}H NMR (400 MHz, $CDCl_3$) δ (ppm): 8.58 (s, 4 H), 8.52 (s, 4 H), 7.94 - 7.88 (m, 8 H), 7.82 (s, 2 H), 7.38 - 7.31 (m, 6 H), 7.02 (d, *J* = 8 Hz, 4 H), 6.89 (s, 2 H), 5.27 (s, 4 H), 4.76 - 4.74 (m, 4 H), 4.68 - 4.64 (m, 4 H), 4.14 - 4.05 (m, 4 H), 1.94 - 1.87 (m, 2 H), 1.40 - 1.27 (m, 16 H), 0.95 - 0.90 (m, 12 H).

^{13}C NMR (125 MHz, $CDCl_3$) δ (ppm): 162.57, 162.08, 160.68, 157.58, 144.93, 143.87, 142.66, 135.46, 135.19, 133.13, 132.99, 132.05, 131.66, 131.34, 129.17, 129.06, 128.96, 128.49, 128.34, 126.94, 125.83, 125.13, 124.17, 124.04, 123.29, 123.22, 122.48, 118.26, 115.01, 62.22, 47.77, 44.66, 40.20, 38.11, 30.79, 28.72, 24.10, 23.21, 14.26, 10.70.

HRMS (ESI): *m/z* calcd for $C_{106}H_{77}BCl_8F_2N_{13}O_{10}^+$ $(M + H)^+$: 2020.3480; Found: 2020.3365.

Synthesis of triad 2

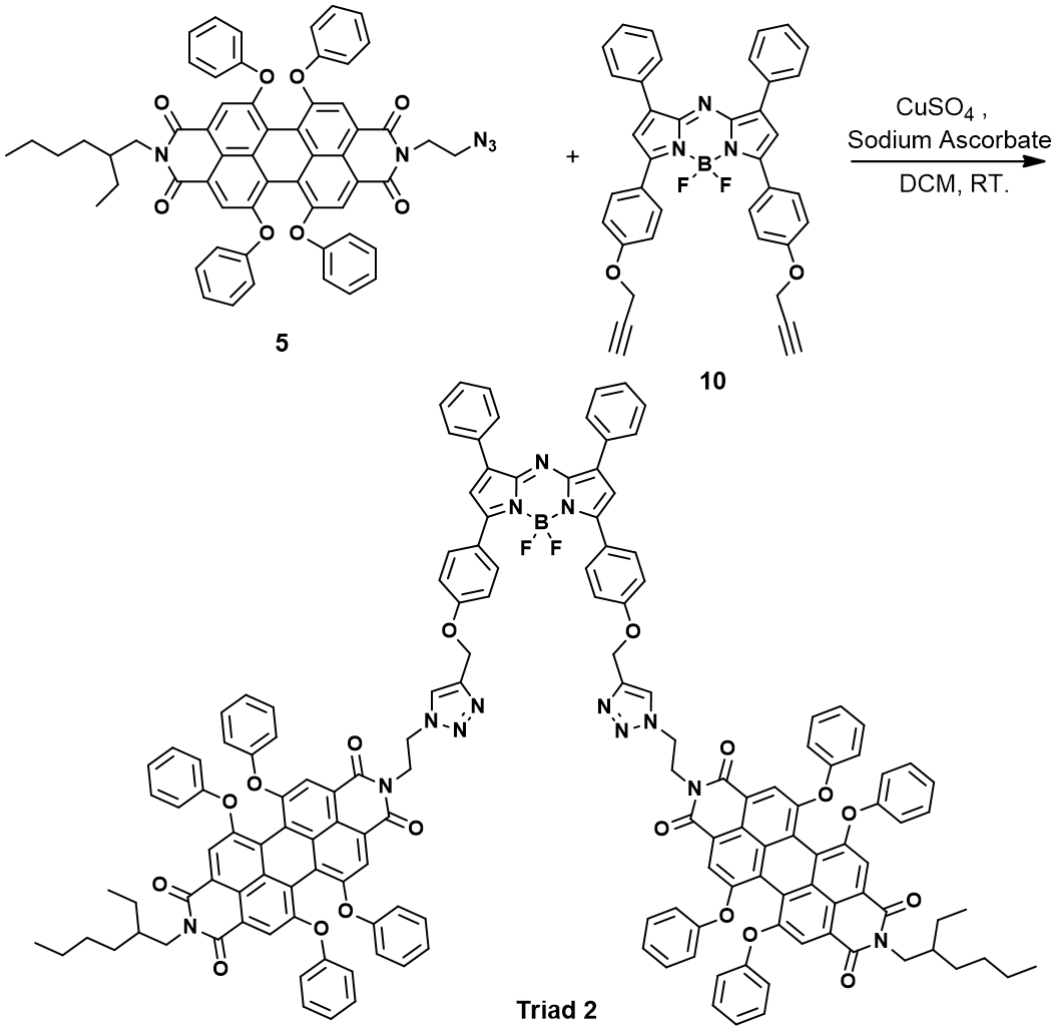

Scheme S5. Synthesis of triad **2**.

PDI compound **5** (39 mg, 0.041 mmol) was dissolved in mixture of DCM, EtOH and water (12:1:1) under nitrogen atmosphere followed by addition of sodium ascorbate (3 mg, 0.015 mmol) and copper sulphate (1.92 mg, 0.007 mmol) to this mixture. After purging the reaction mixture with nitrogen for 15 minutes, compound **10** (10 mg, 0.016 mmol) was added and the reaction mixture was stirred for 24 h at room temperature. After the completion of reaction, mixture was extracted with DCM, the organic layer was dried over sodium sulphate and solvent was removed under reduced pressure. The crude was purified by column chromatography DCM/EA (3/1) as eluent and a purple solid compound (triad **2**) was obtained.

Yield: 33 mg (80 %).

^{1}H NMR (500 MHz, $CDCl_3$) δ (ppm): 8.15 (s, 4 H), 8.11 (s, 4 H), 8.01 (t, J = 5 Hz, 8 H), 7.71 (s, 2 H), 7.45 - 7.39 (m, 6 H), 7.26 - 7.22 (m, 16 H), 7.09 (t, J = 6.5 Hz, 8 H), 7.01 - 6.98 (m, 6 H), 6.91 (d, J = 10 Hz, 16 H), 5.21 (s, 4 H), 4.71 - 4.68 (m, 4 H), 4.60 - 4.57 (m, 4 H), 4.05 - 3.95 (m, 4 H), 1.86 - 1.81 (m, 2 H), 1.33 - 1.22 (m, 16 H), 0.89 - 0.83 (m, 12 H).

^{13}C NMR (125 MHz, $CDCl_3$) δ (ppm): 163.72, 163.19, 160.64, 158.12, 156.23, 155.77, 155.42, 155.29, 145.42, 143.98, 143.91, 133.02, 132.87, 132.51, 131.75, 131.71, 130.12, 129.39, 128.67, 124.79, 124.75, 124.67, 123.51, 122.96, 121.87, 121.27, 120.42, 120.21, 120.05, 119.98, 119.83, 119.61, 115.14, 62.26, 47.96, 44.46, 39.93, 38.20, 30.92, 28.89, 24.18, 23.19, 14.24, 10.74.

HRMS (ESI): *m/z* calcd for $C_{154}H_{117}BF_2N_{13}O_{18}^{+}$ $(M+H)^{+}$: 2484.8695; Found: 2484.8560.

We also attempted the synthesis of a triad similar to triad **1** without bay-substitution at the PDI subchromophore and the triad product was formed as indicated from TLC analysis in DCM/MeOH solvent mixture and the purple colour of the final compound. However, the compound was not soluble in common organic solvents due to unsubstituted bay positions in PDIs and thus, could not be purified by column chromatography and analysed by NMR.

3. NMR spectra

^{1}H NMR spectra of Compound 2 in $CDCl_3$

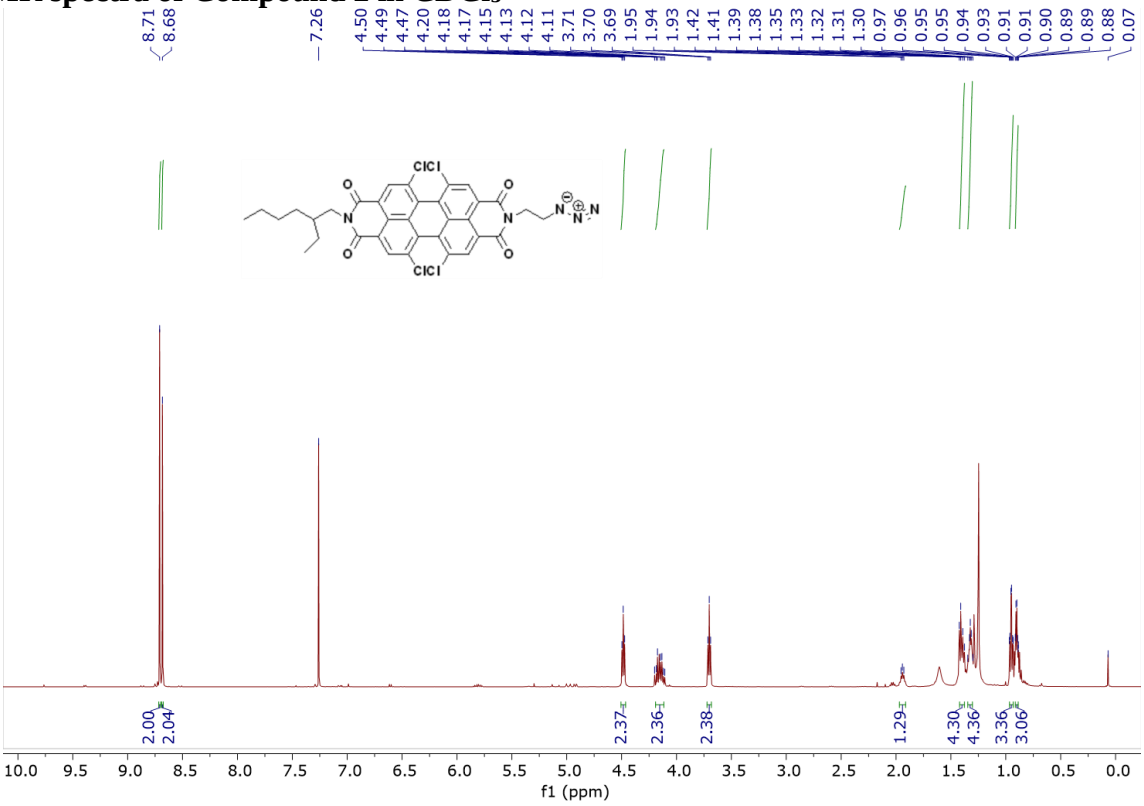

^{13}C NMR spectra of Compound 2 in $CDCl_3$

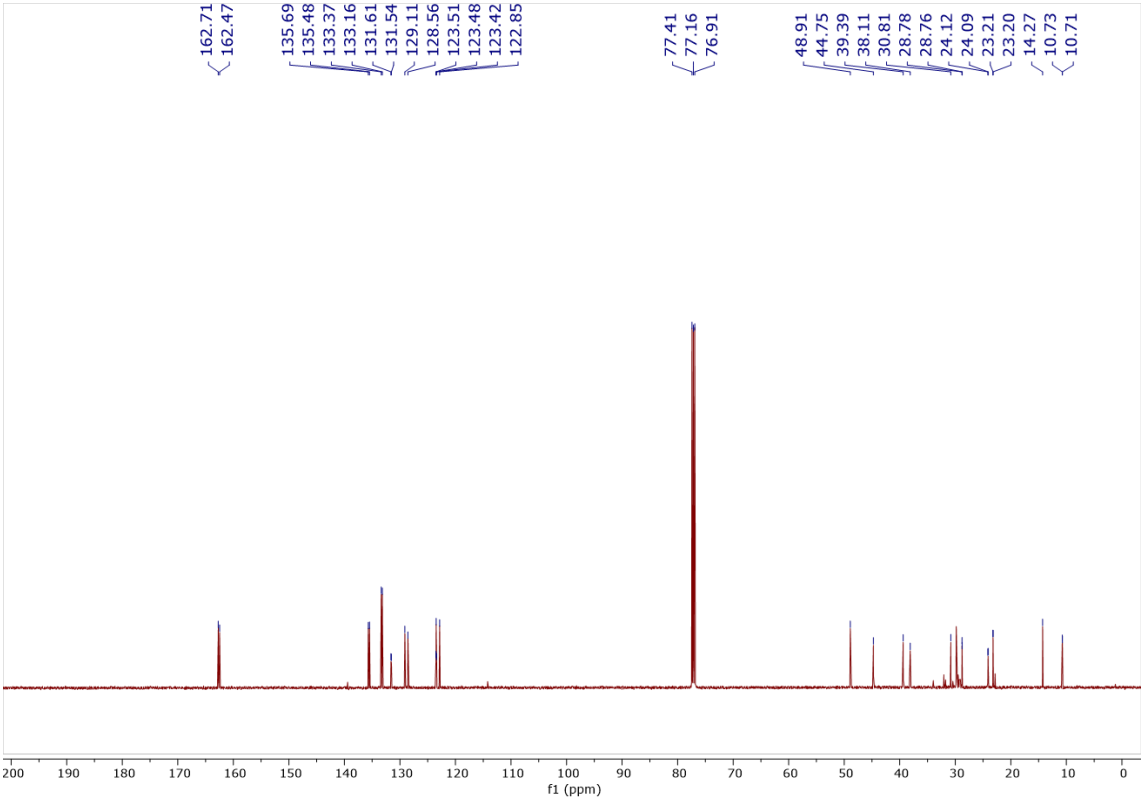

^{1}H NMR spectra of Compound 3 in $CDCl_3$

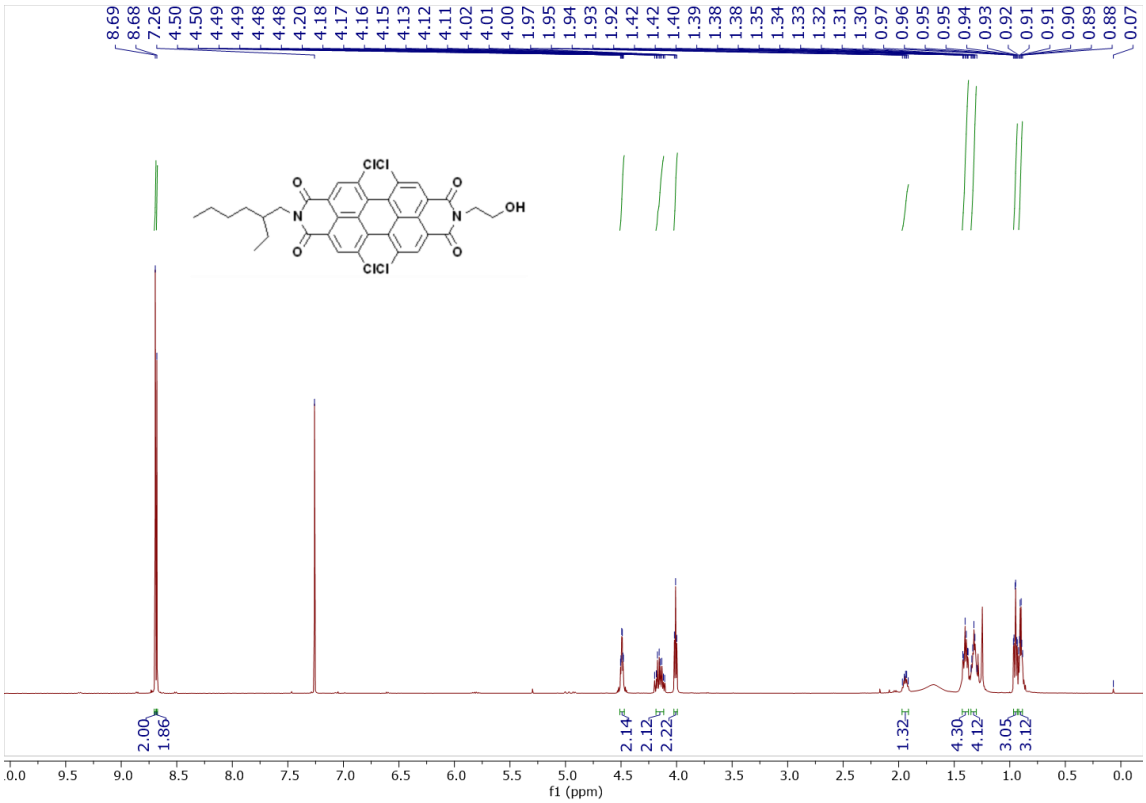

^{13}C NMR spectra of Compound 3 in $CDCl_3$

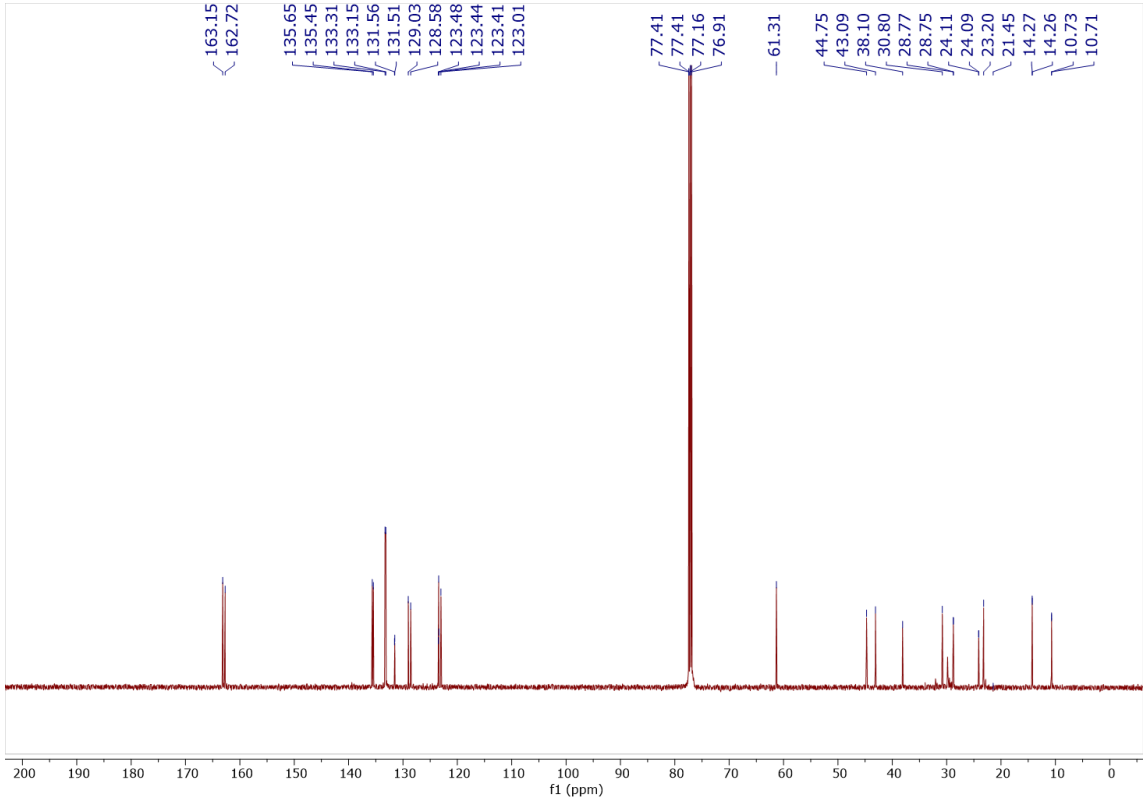

^{1}H NMR spectra of Compound 4 in $CDCl_3$

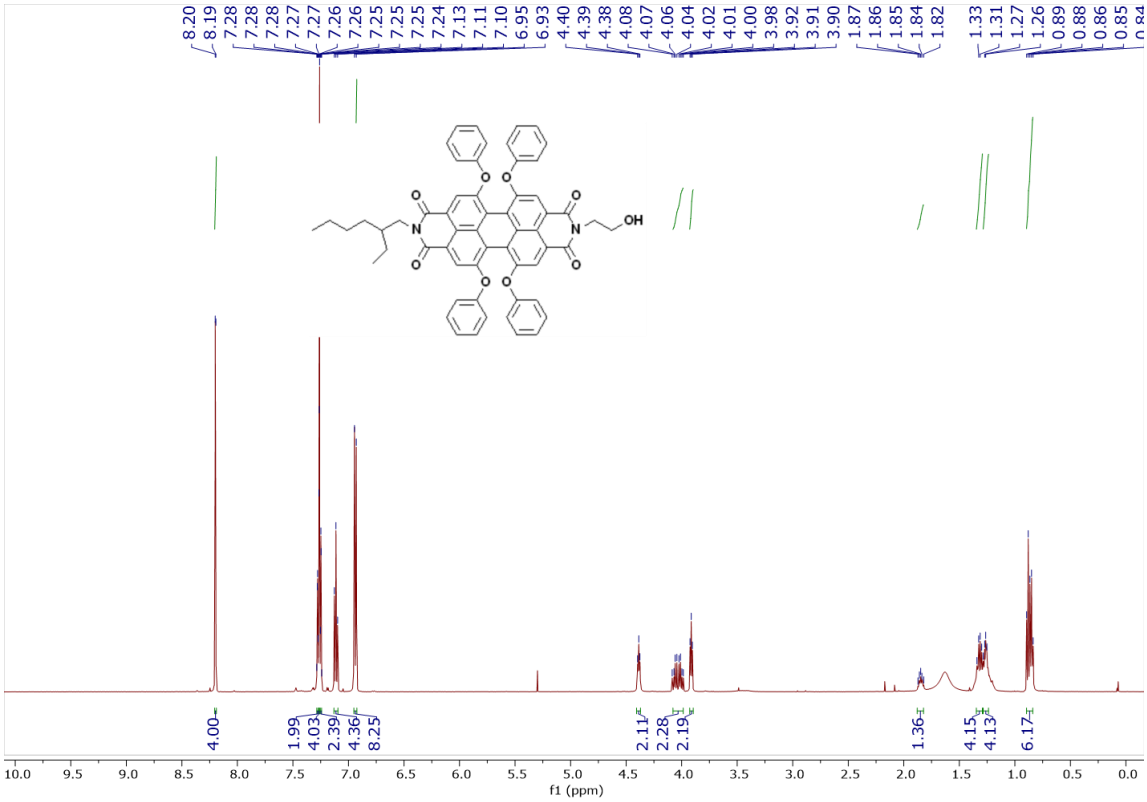

^{13}C NMR spectra of Compound 4 in $CDCl_3$

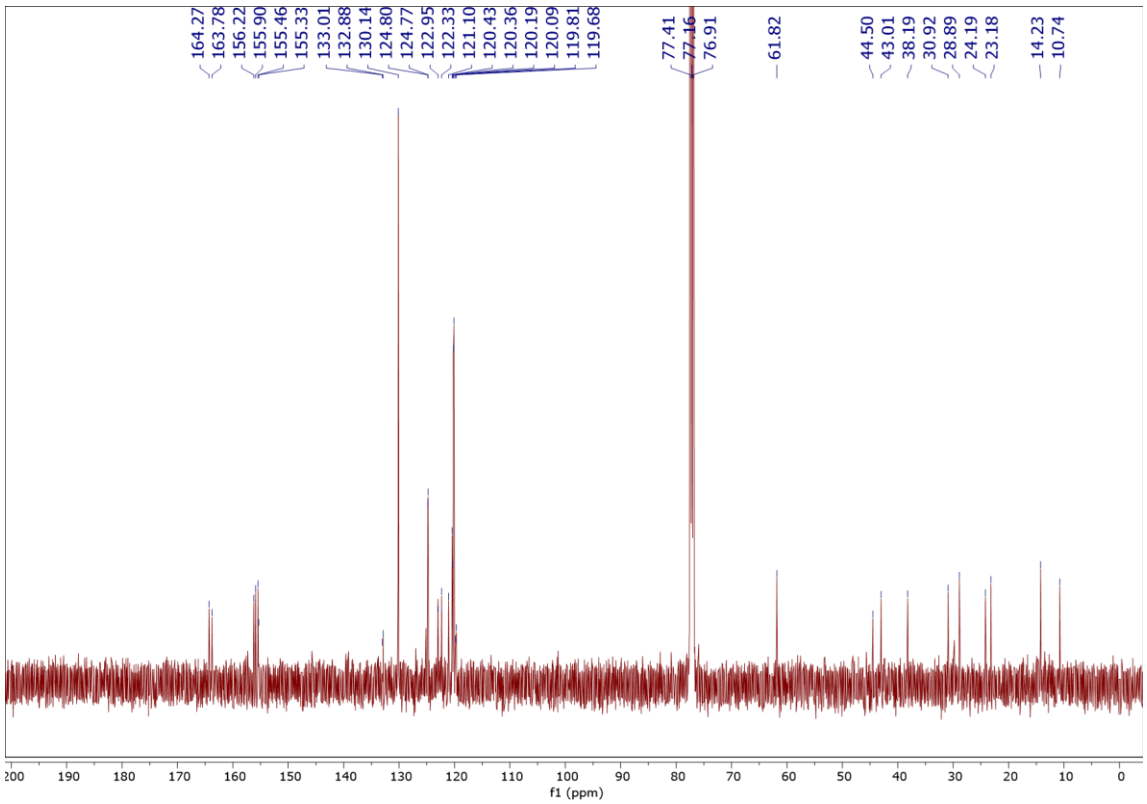

^{1}H NMR spectra of Compound 5 in $CDCl_3$

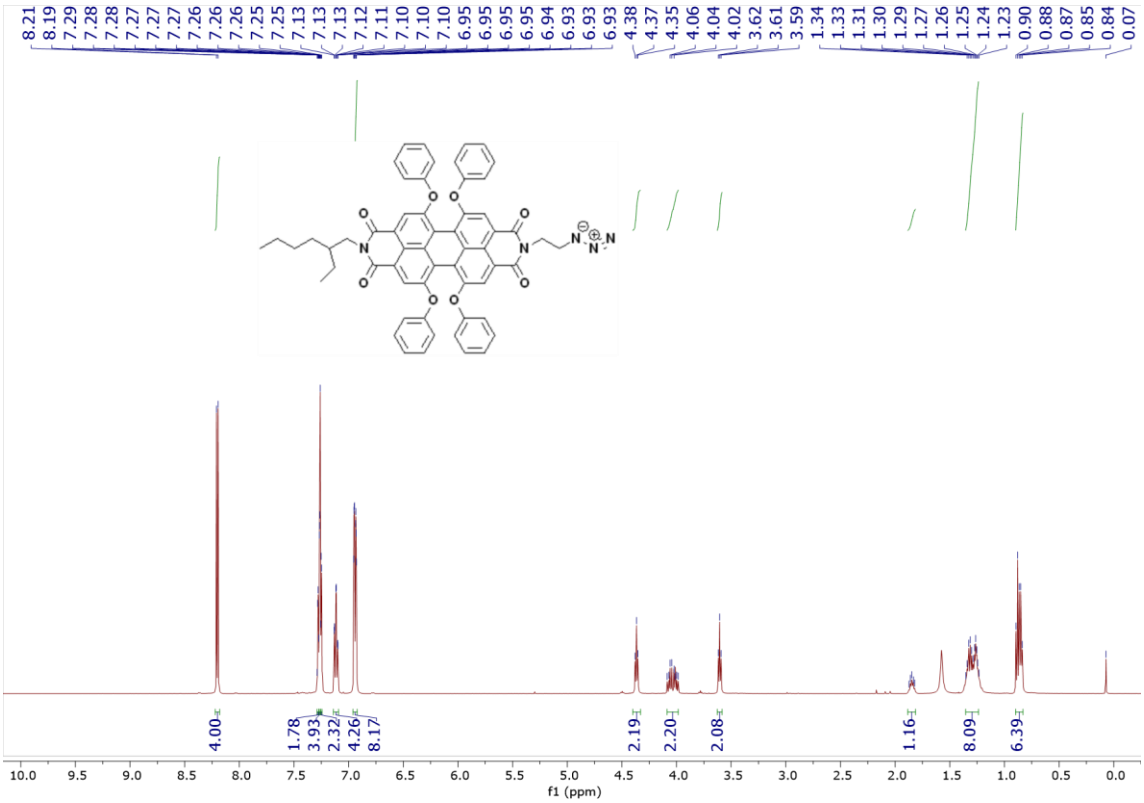

^{13}C NMR spectra of Compound 5 in $CDCl_3$

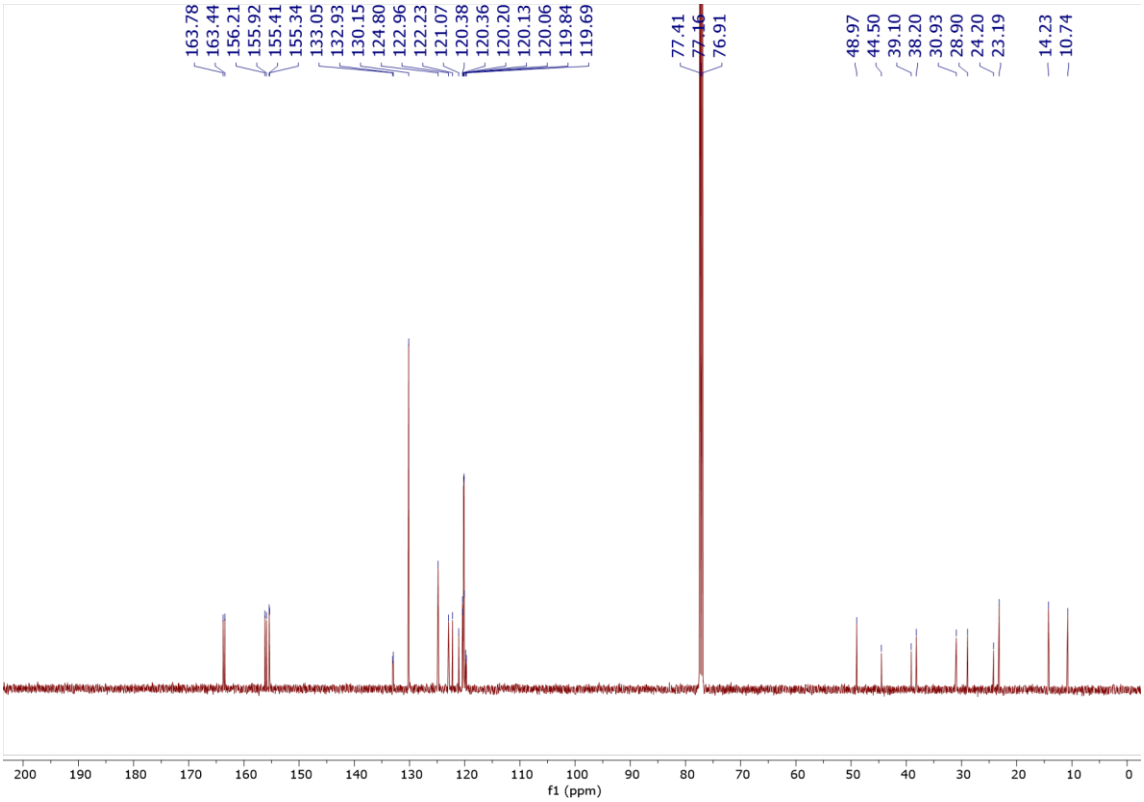

^{1}H NMR spectra of Compound 6 in CD_3OD

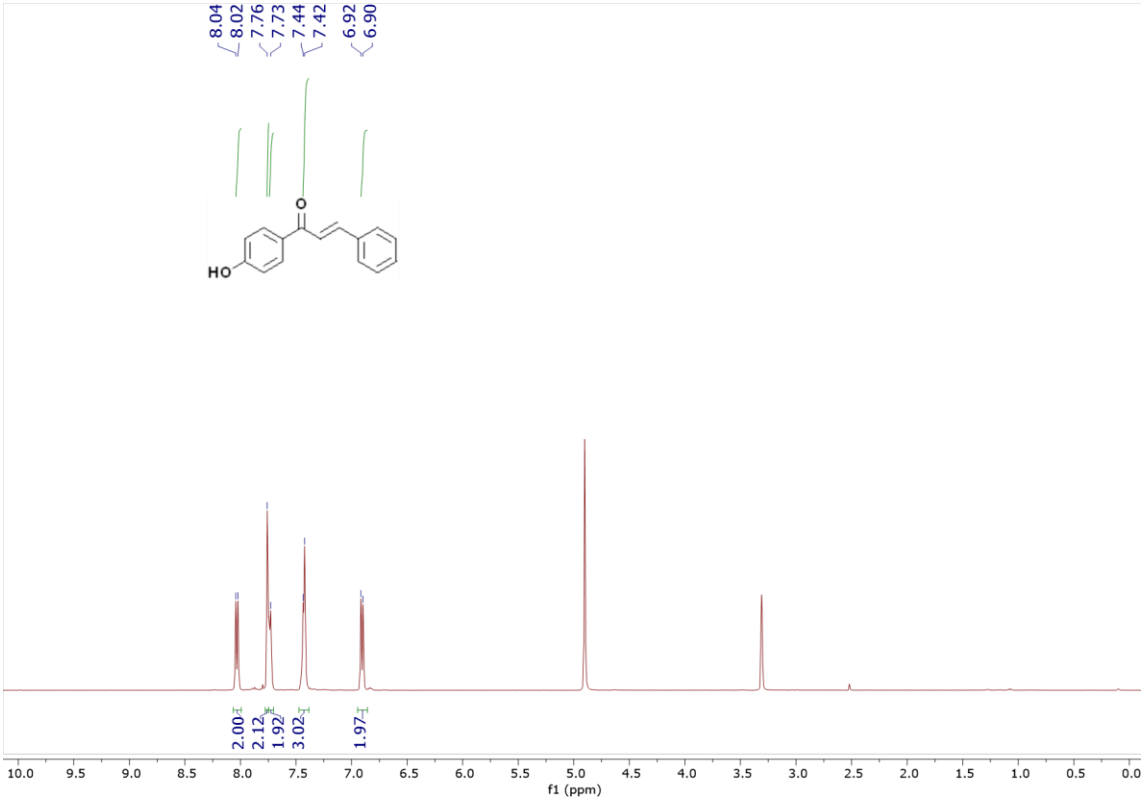

^{1}H NMR spectra of Compound 7 in $CDCl_3$

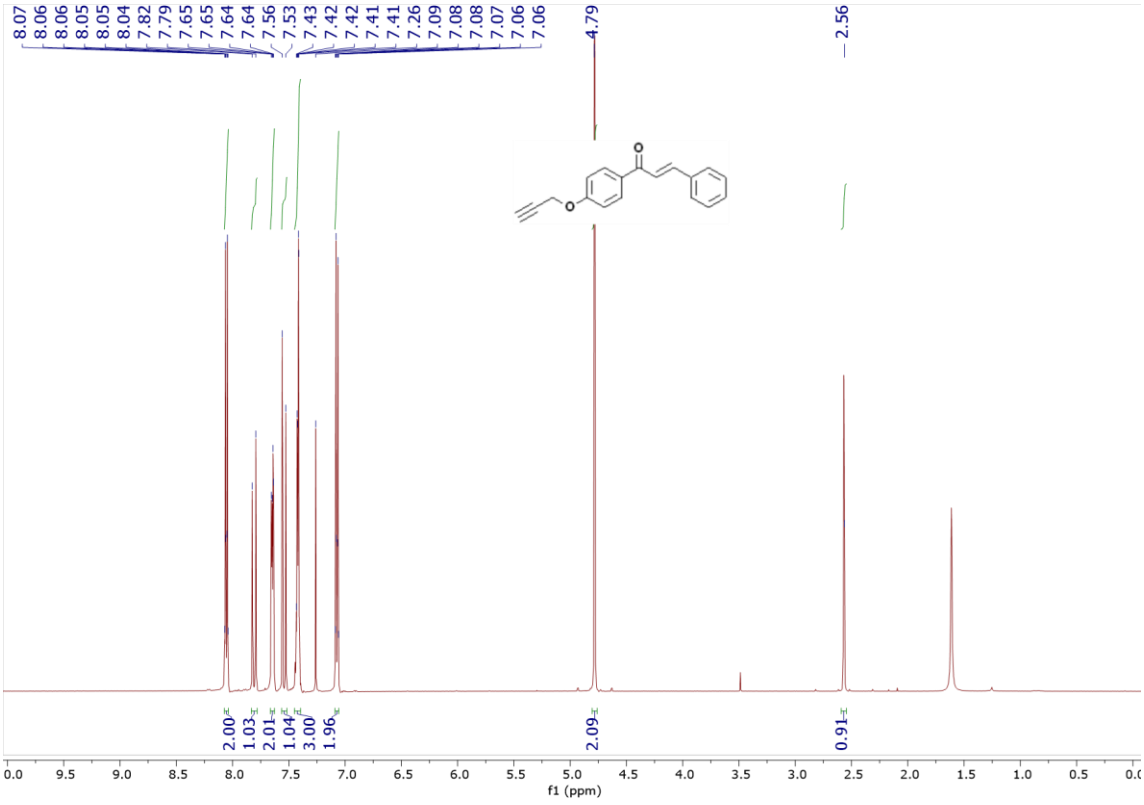

^{1}H NMR spectra of Compound 8 in $CDCl_3$

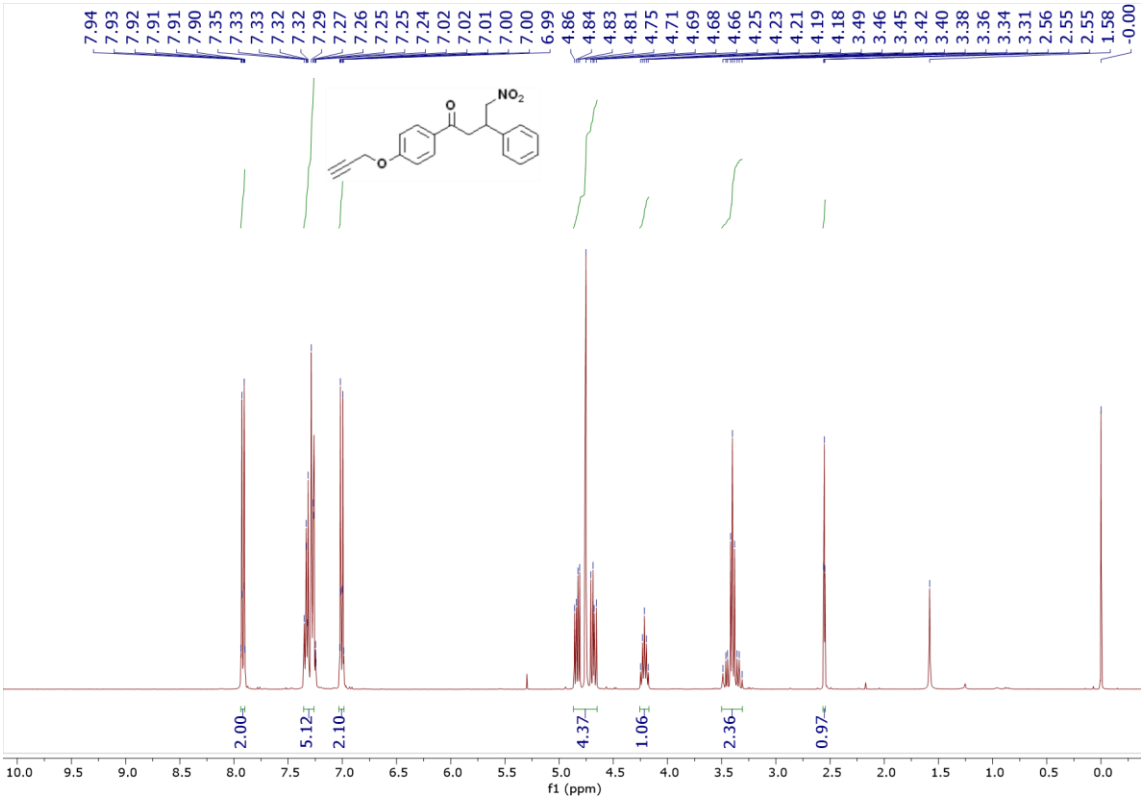

^{1}H NMR spectra of Compound 10 in $CDCl_3$

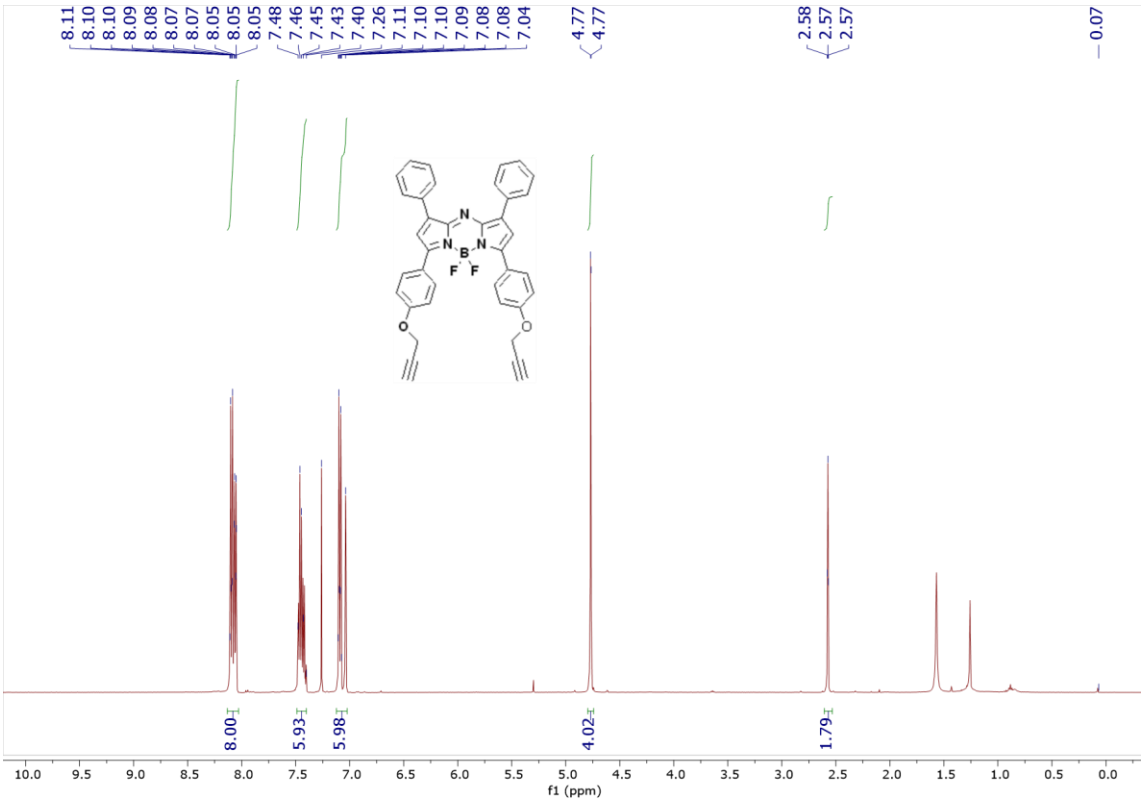

^{13}C NMR spectra of Compound 10 in $CDCl_3$

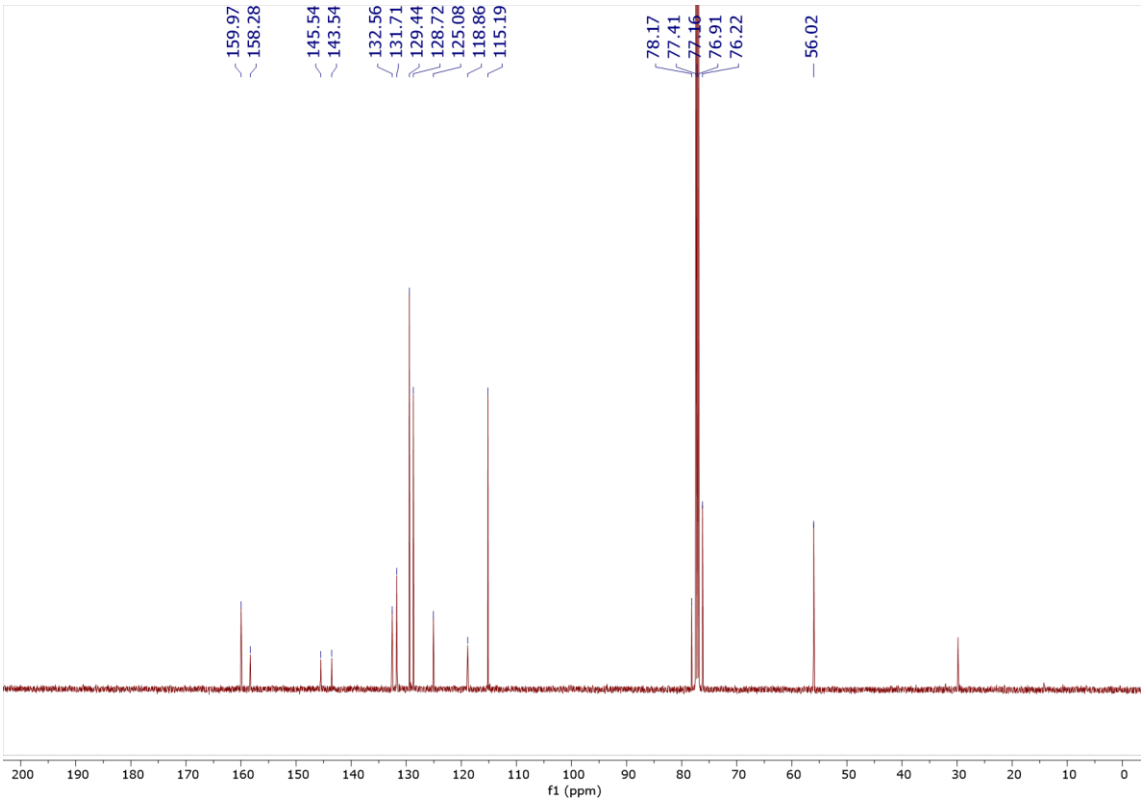

Triad 1

^{1}H NMR spectra of triad 1 in $CDCl_3$

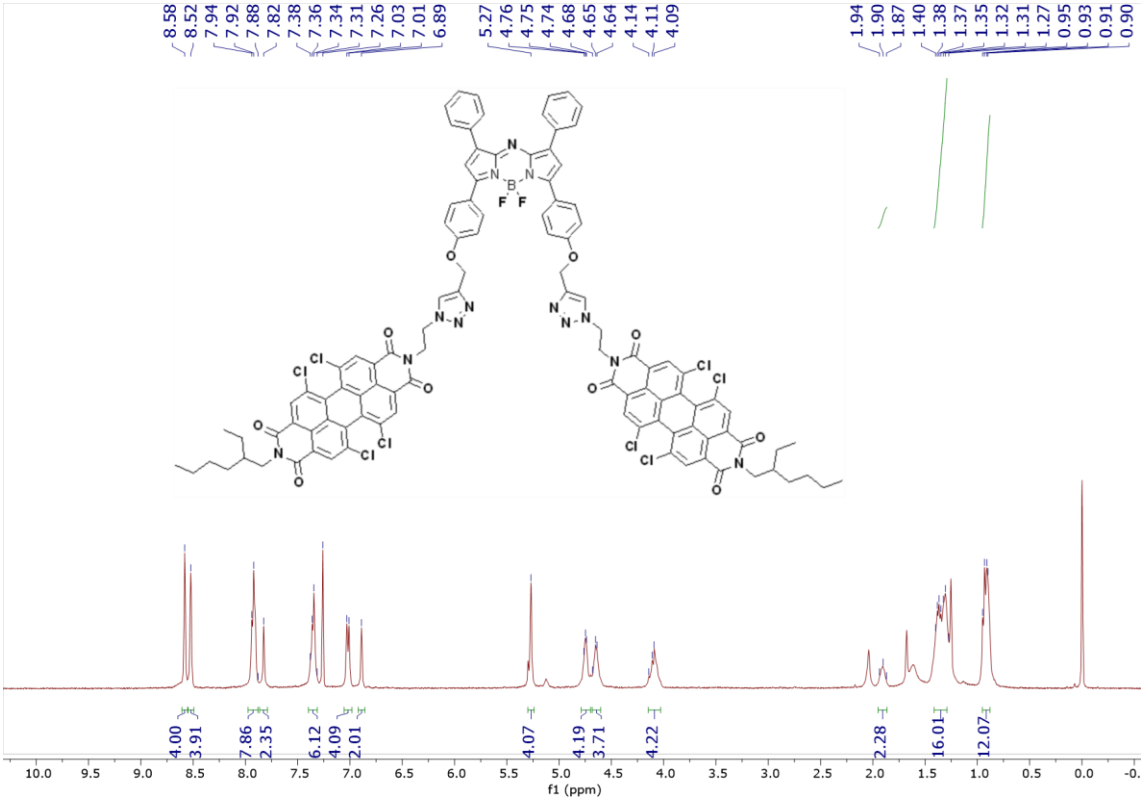

^{13}C NMR spectra of triad 1 in $CDCl_3$

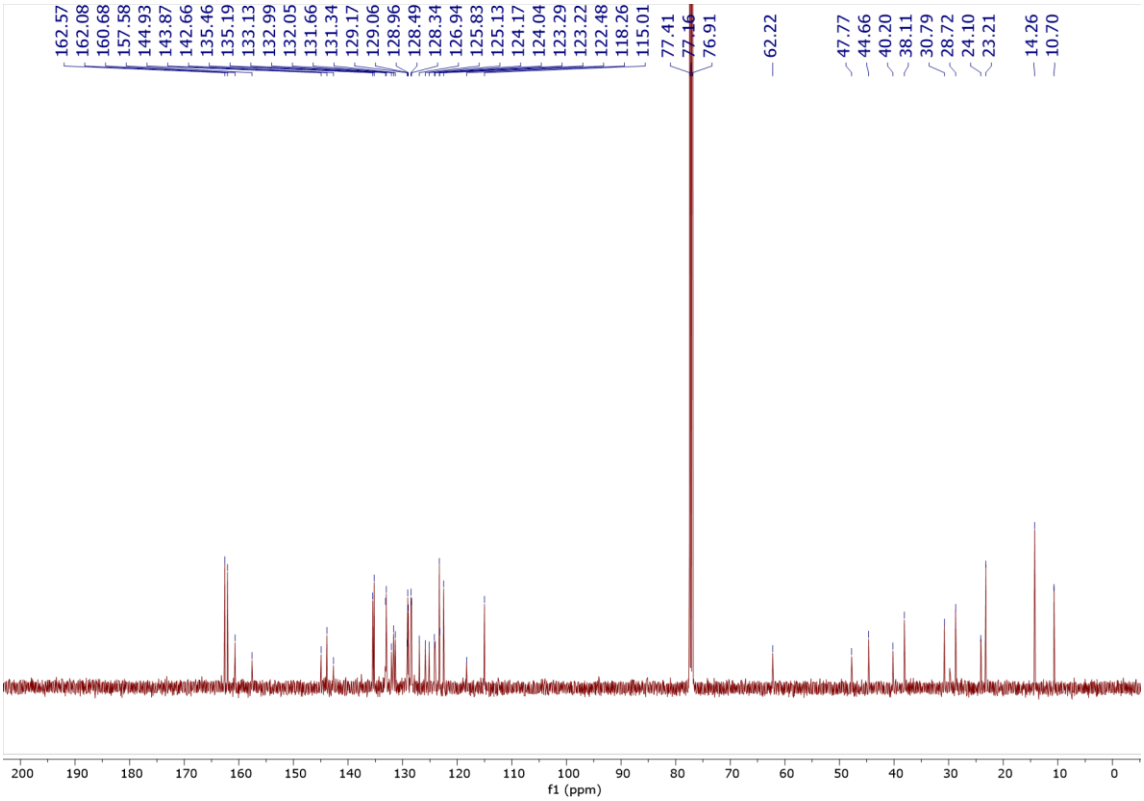

Triad 2

^{1}H NMR spectra of triad 2 in $CDCl_3$

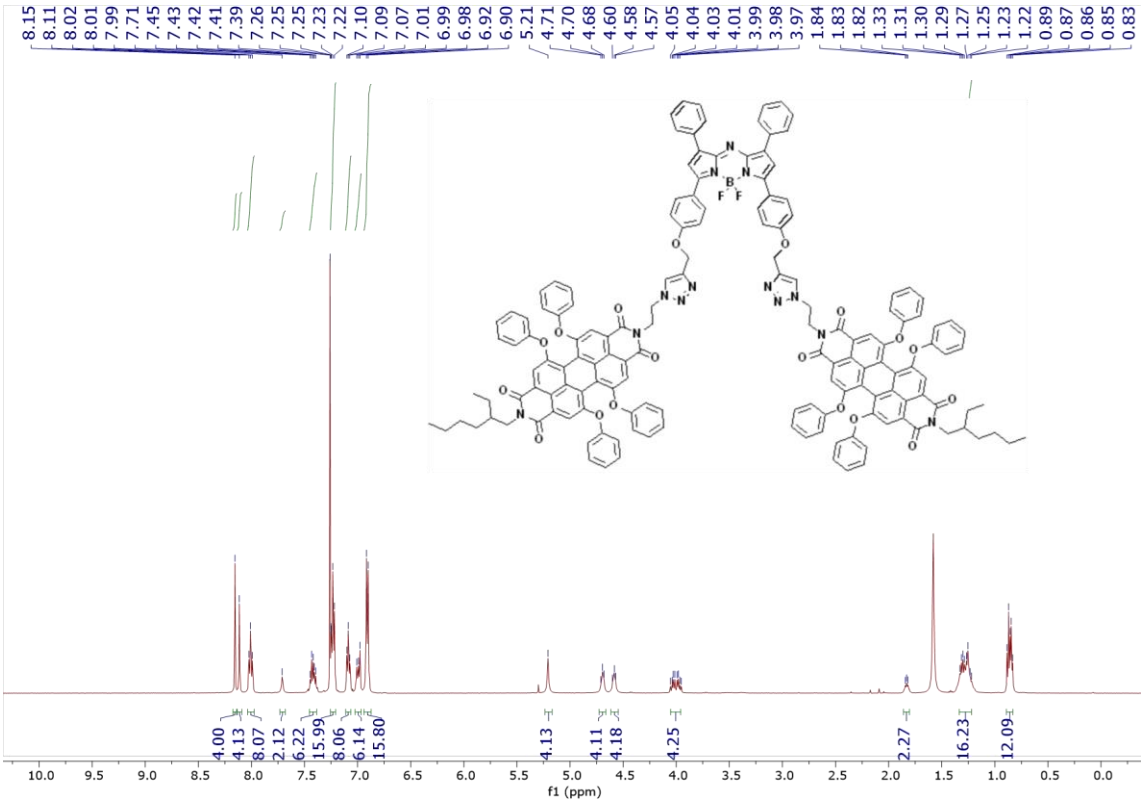

^{13}C NMR spectra of triad 2 in $CDCl_3$

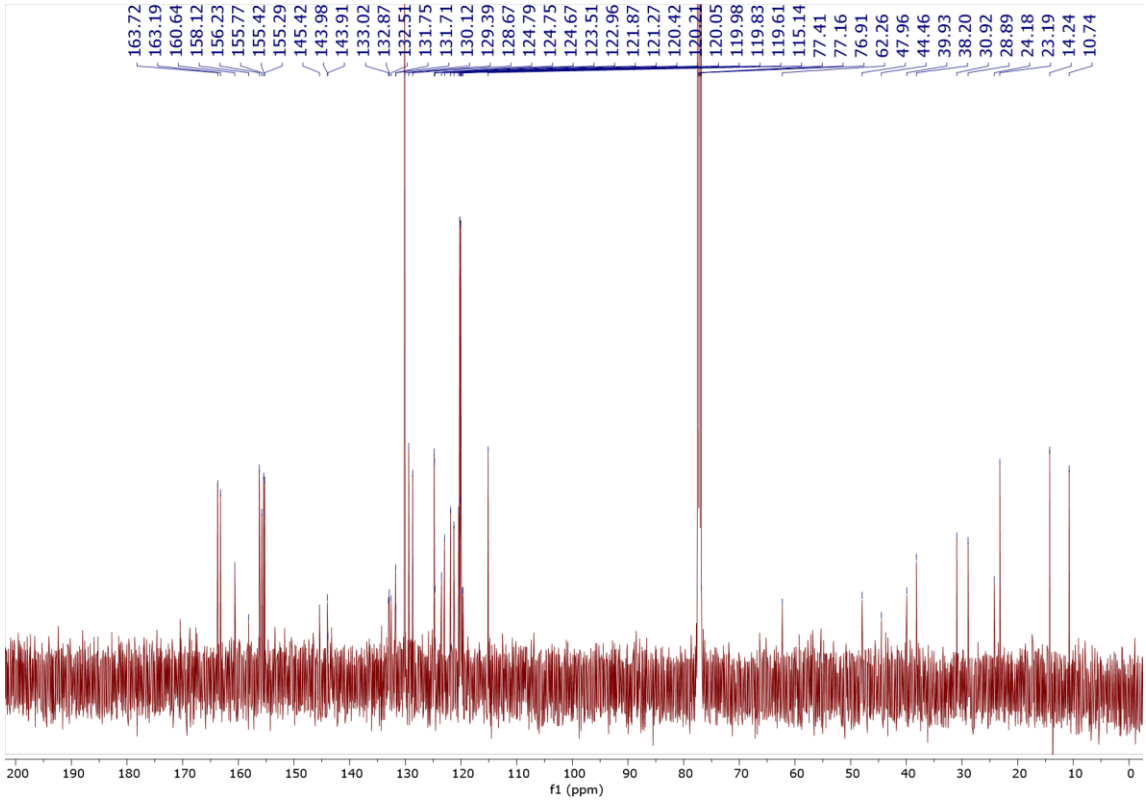

4. Photophysical Properties

Thin Film UV/Vis spectra

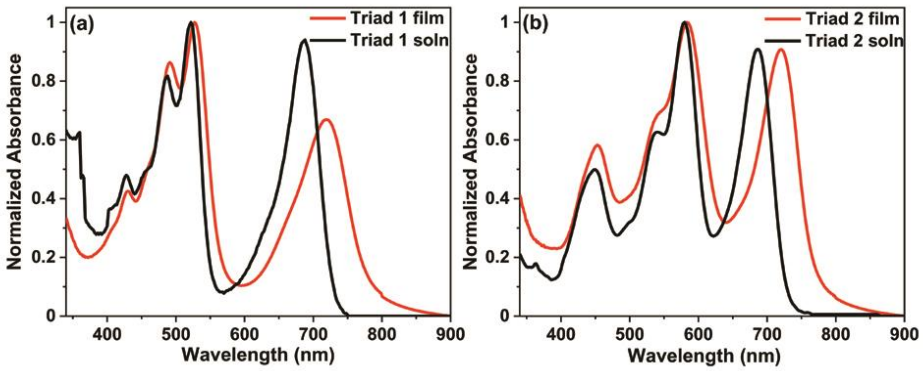

Figure S1. Thin film UV/Vis spectra for (a) triad **1** and (b) triad **2** spin-coated from $CHCl_3$ solutions (2 mg/mL) onto quartz substrates at ~ 500 rpm.

Calculation of energy transfer efficiency EET

EET was calculated according to equations (3) and (4)[S9]

$EET = 1 - \Phi_{DA}/\Phi_D$ (3)

$EET = 1 - \tau_{DA}/\tau_D$ (4)

From excitation spectrum EET was calculated by taking the peak-intensity ratios of the absorption and excitation spectrum.[S10, S11]

For triad **1** the intensity ratio of PDI to aza-BODIPY band were found to be 1.09 from excitation spectrum (Fig. 4a) and 1.06 from absorption spectrum (Fig. 2a) which indicates 100 % ETE.
For triad **2** the intensity ratio of PDI to aza-BODIPY band were found to be 1.17 from excitation spectrum (Fig. 4b) and 1.10 from absorption spectrum (Fig. 2b) which indicates 100 % ETE.

Table S1. Fluorescence quantum yields of **3**, **4**, triads **1** and **2** obtained by relative method of fluorescence quantum yield.

Compound	**Absorbance**			**Integrated fluorescence intensity**			**Quantum Yield** $\Phi = \Phi_R(I/I_R)(A_R/A)(\lambda_{ex.R}/\lambda_{ex})(n^2/n_R^2)$		**ETE = 1 - Φ_{DA} / Φ_D**
	1	2	3	1	2	3	ϕ_i	ϕ_{avg}	
3	0.0223	0.0317	0.0589	182.30	260.20	510.16	1.02 1.02 1.03	~ 1	
4	0.0258	0.0383	0.0542	92.92	135.52	175.30	0.80 0.83 0.78	~ 0.81	
Triad **1**	0.0341	0.0558	0.0727	4.45	4.45	5.96	0.016 0.009 0.009	~ 0.01	~ 99 %
Triad **2**	0.0206	0.0288	0.0334	1.69	2.36	2.90	0.018 0.019 0.021	~ 0.01	~ 98 %
Rhodamine 6G (ethanol)	0.0295	0.0474	0.0617	276.90	443.77	602.31		0.95 (reported)	
Lumogen® F Red 305 (in $CHCl_3$)	0.0315	0.0394	0.0454	135.19	160.11	178.19		0.96 (reported)	

Table S2. Fluorescence lifetime analysis of **3**, **4**, **10**, triads **1** and **2** at different excitation and emission wavelengths.

Compound	**λ_{ex} (nm)**	**λ_{em} (nm)**	**τ_1 (α_1) (ns)**	**τ_2 (α_2) (ns)**	**τ_3 (α_3) (ns)**	**τ_{avg} (ns)**	**χ^2**	**ETE = 1- τ_{DA} / τ_D**
3	510	550	5.12 (1.00)	-	-	5.12	1.00	
4	590	612	6.33 (1.00)	-	-	6.33	1.03	
Triad **1**	510	550	0.41 (0.51)	4.45 (0.49)	-	2.39	1.10	~ 53 %
Triad **2**	590	614	2.04 (0.53)	6.19 (0.21)	5.92 (0.26)	2.74	1.12	~ 56 %

Overlay of emission spectra of energy donor and absorption spectra of energy acceptor for triads 1 and 2

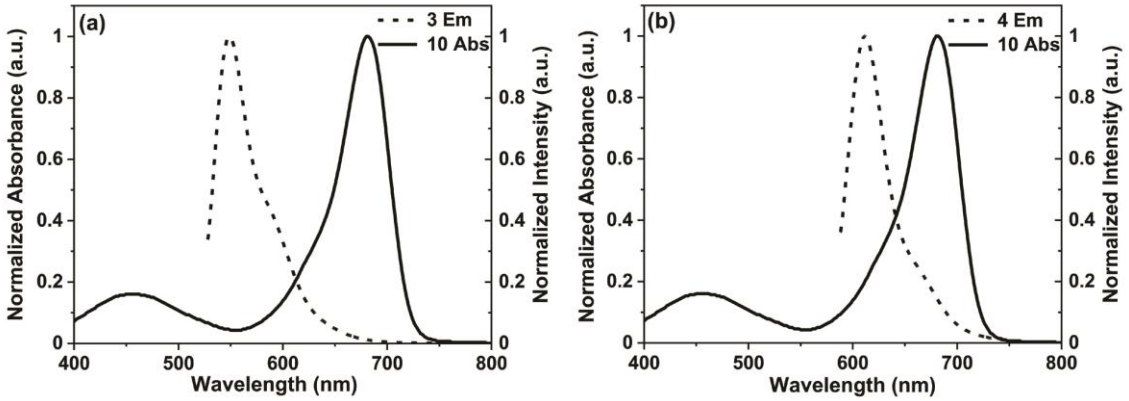

Figure S2. (a) Overlap of the emission of **3** with the absorption of **10** (b) Overlap of the emission of **4** with the absorption of **10** in $CHCl_3$.

Solvatochromism

The solvatochromism studies of triads**1** and **2** and corresponding reference aza-BODIPY **10** and PDIs **3** and **4** compounds were performed in six different solvents.

Table S3. Solvatochromism study of **3**, **4**, **10**, triad **1** and triad **2** in different solvents.

Compound	**Benzonitrile**		**DCM**		**THF**		**Chlorobenzene**		**Chloroform**		**1,4-Dioxane**	
	λ_{abs} (nm)	λ_{em} (nm)	λ_{abs} (nm)	λ_{em} (nm)	λ_{abs} (nm)	λ_{em} (nm)	λ_{abs} (nm)	λ_{em} (nm)	λ_{abs} (nm)	λ_{em} (nm)	λ_{abs} (nm)	λ_{em} (nm)
3	523	551	519	547	514	543	524	552	520	550	515	543
4	576	608	573	607	564	595	575	607	580	612	563	595
10	691	721	680	712	687	717	689	718	682	714	685	714
Triad **1**	524, 698	549, 726 (λ_{exc} = 524 nm)	520, 688	547, 715 (λ_{exc} =520 nm)	516, 695	545, 721 (λ_{exc} =520 nm)	524, 694	552, 721 (λ_{exc} = 524 nm)	520 , 688	550, 717 (λ_{exc}= 520 nm)	517, 692	545, 717 (λ_{exc} =517 nm)
Triad **2**	580, 698	611, 723 (λ_{exc} = 580 nm)	575, 687	607, 719 (λ_{exc}= 575 nm)	569, 693	595, 722 (λ_{exc}= 569 nm)	577, 695	609, 723 (λ_{exc}= 577 nm)	580, 688	614, 717 (λ_{exc} = 580 nm)	569, 692	598, 719 (λ_{exc} = 569 nm)

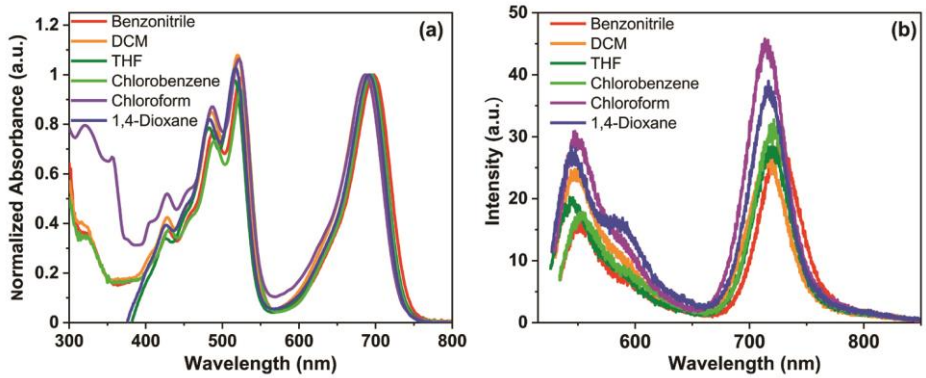

Figure S3. (a) UV/Vis and (b) fluorescence spectra of triad **1** (c ~ 2 μM) in different solvents.

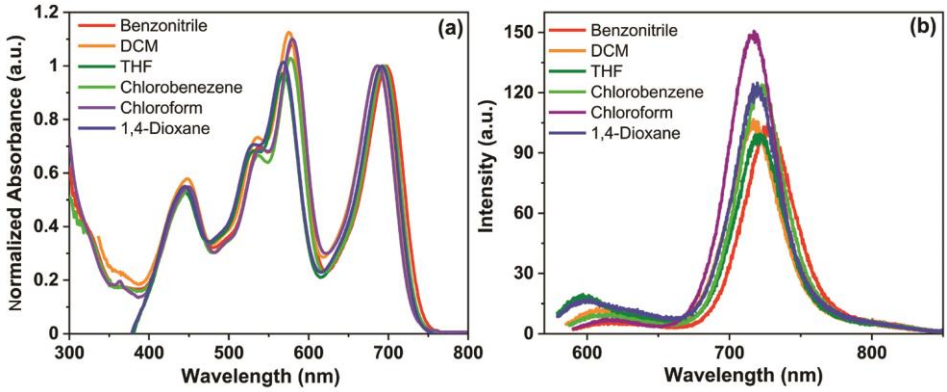

Figure S4. (a) UV/Vis and (b) fluorescence spectra of triad **2** (c ~ 2 μM) in different solvents (In chloroform intensity /1.6).

The absorption maxima and emission maxima for both triads **1** and **2** showed negligible shifts in six solvents of different polarities as presented in Table S3 suggesting solvent polarity has little influence on ground state and excited state properties for the triads. The observation further indicates the absence of photoinduced electron transfer in triads **1** and **2** in different solvents.[S12] Furthermore, fluorescence studies were performed for triads **1** and **2** (Figures S5 and S6) along with their donor subchromophores in the same six solvents and their energy transfer efficiencies were calculated (Table S4).

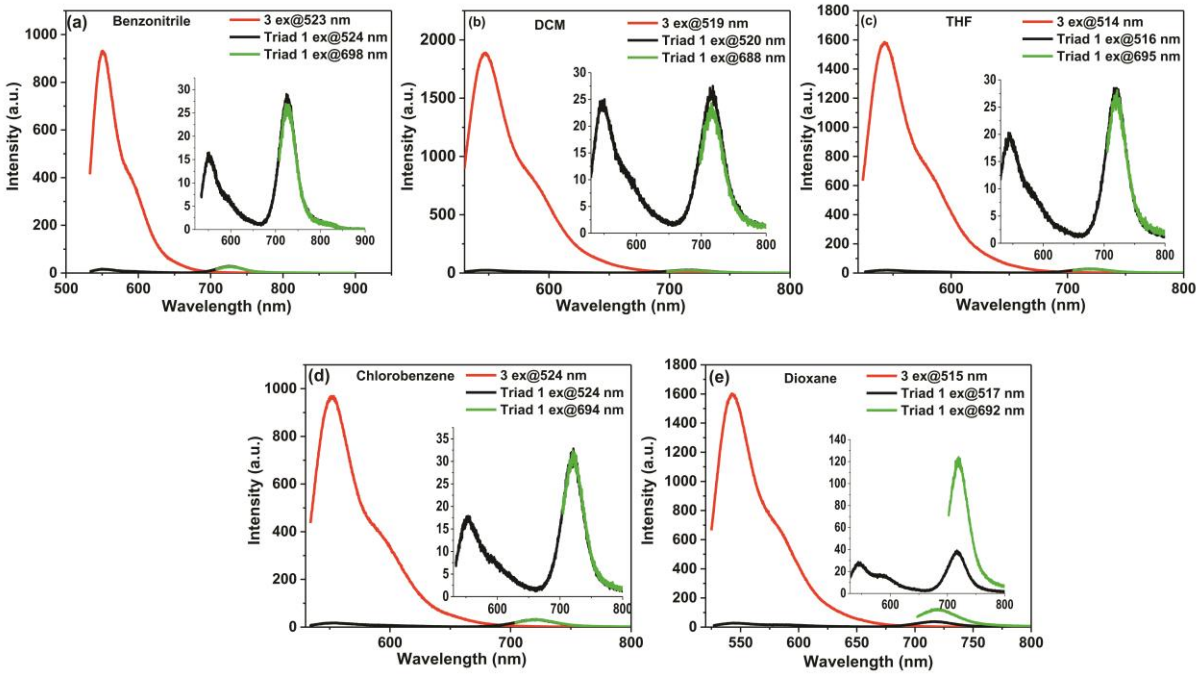

Figure S5. Fluorescence spectra of **3** and triad **1** in (a) Benzonitrile, (b) DCM, (c) THF, (d) Chlorobenzene and (e) 1,4-dioxane (c ~ 2×10^{-6} M).

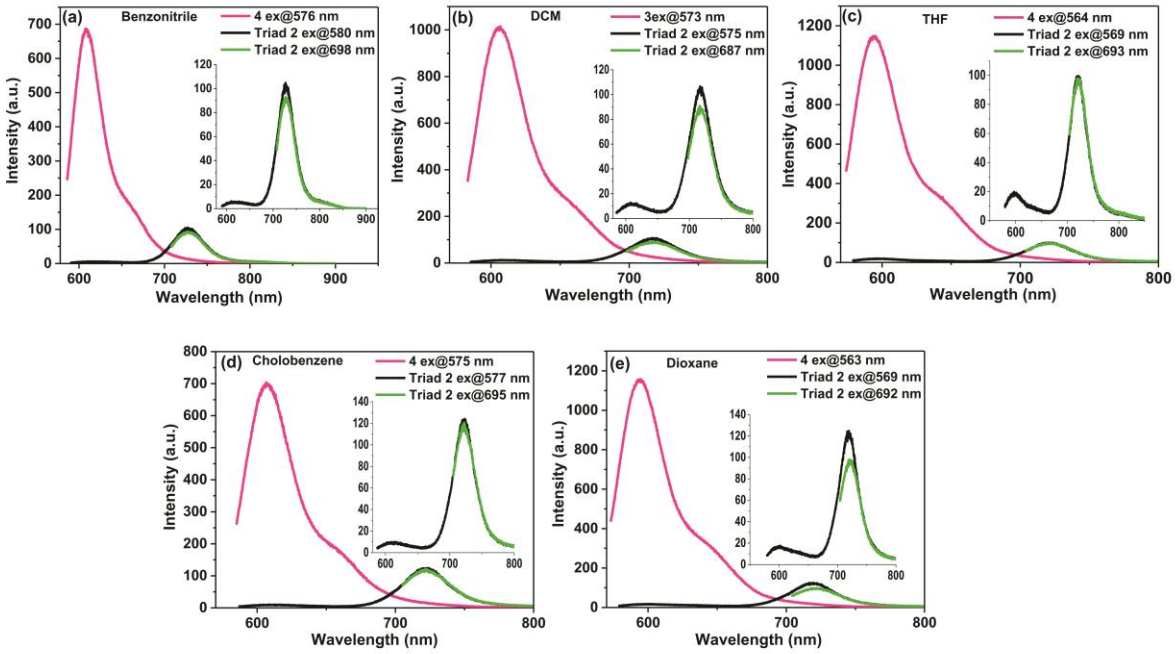

Figure S6. Fluorescence spectra of **4** and triad **2** in (a) Benzonitrile, (b) DCM, (c) THF, (d) Chlorobenzene and (e) 1,4-dioxane (c ~ 2×10^{-6} M).

The fluorescence spectra of triads **1** and **2** were recorded by exciting at both donor and acceptor absorption band in different solvents and energy transfer efficiencies (ETEs) were calculated based on fluorescence intensity of pure donor (F_D) and the decay of donor in triads (F_{DA}) by using equation 5[S9].

$$ETE = 1- F_{DA}/F_D \qquad (5)$$

Table S4. Energy transfer efficiencies (ETE) of triad **1** and triad **2** in different solvents.

Compound	Benzonitrile	DCM	THF	Chlorobenzene	Chloroform	1,4-Dioxane
Triad 1	~ 98%	~ 99%	~ 99%	~ 98%	~ 98%	~ 98%
Triad 2	~ 99%	~ 99%	~ 98%	~ 98%	~ 99%	~ 99%

5. Electrochemical Properties

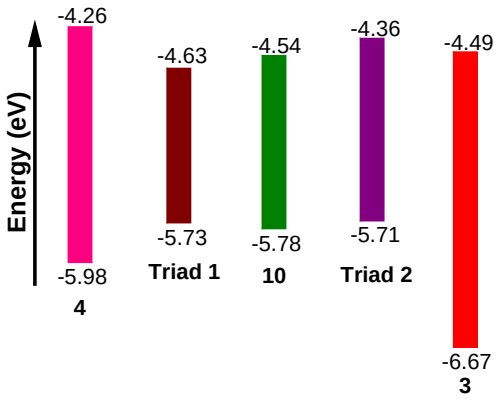

Figure S7. Alignment of frontier molecular orbital energy levels (in eV) obtained from cyclic voltammetry measurements for reference subchromophores **3**, **4** and **10** and triads **1** and **2**.

Since the PDI compound **3** doesn't show any oxidation process, energy donor in case of triad **1**, the Gibbs free energy for photoinduced electron transfer (ΔG_{CS}) from donor to acceptor for triad **1** was not calculated.

6. Charge Carrier Mobilities and Powder X-ray Diffraction

Table S5. Device optimizations and charge carrier mobilities performed on five devices each provide the average mobilities.

Device No.	μ_e (cm^2/V.s)	
	Triad 1	**Triad 2**
1	1.25×10^{-3}	4.82×10^{-3}
2	1.47×10^{-3}	1.69×10^{-3}
3	2.09×10^{-3}	4.70×10^{-3}
4	4.93×10^{-3}	5.68×10^{-3}
5	-	3.10×10^{-3}
Average	2.44×10^{-3}	4.00×10^{-3}
Std. Dev.	1.70×10^{-3}	1.60×10^{-3}
Final	$(2.44 \pm 1.70) \times 10^{-3}$	$(4.00 \pm 1.60) \times 10^{-3}$

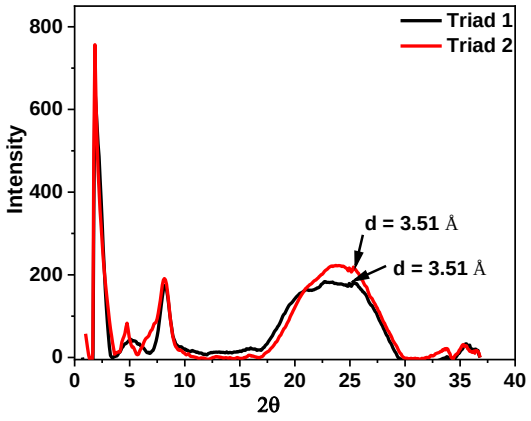

Figure S8. Small angle X-ray diffraction patterns of powder samples of triads **1** and **2**.

7. Metal Ion Sensing

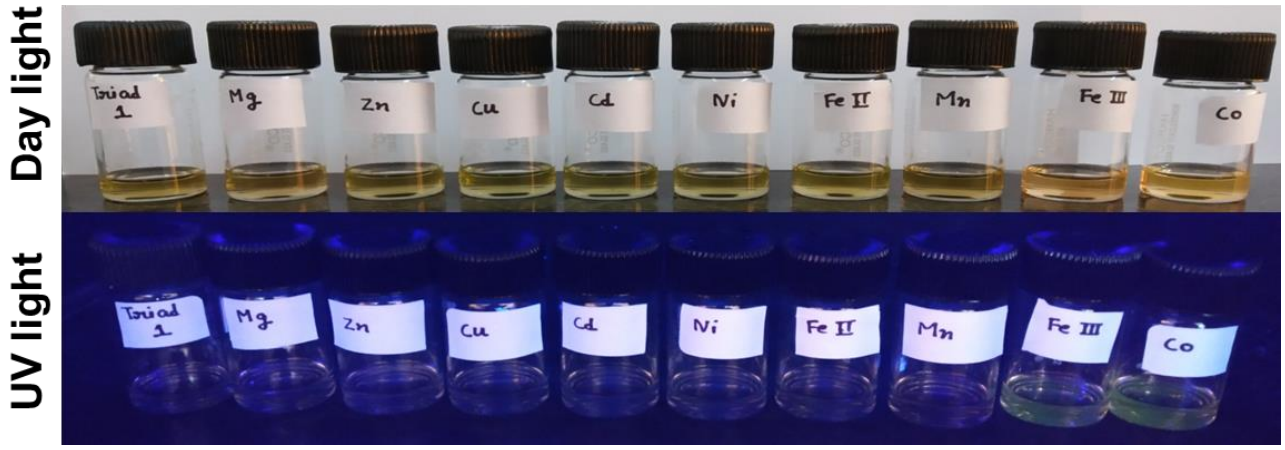

Figure S9. Images of triad **1** with addition of different cations under normal light (top) and under UV light (bottom).

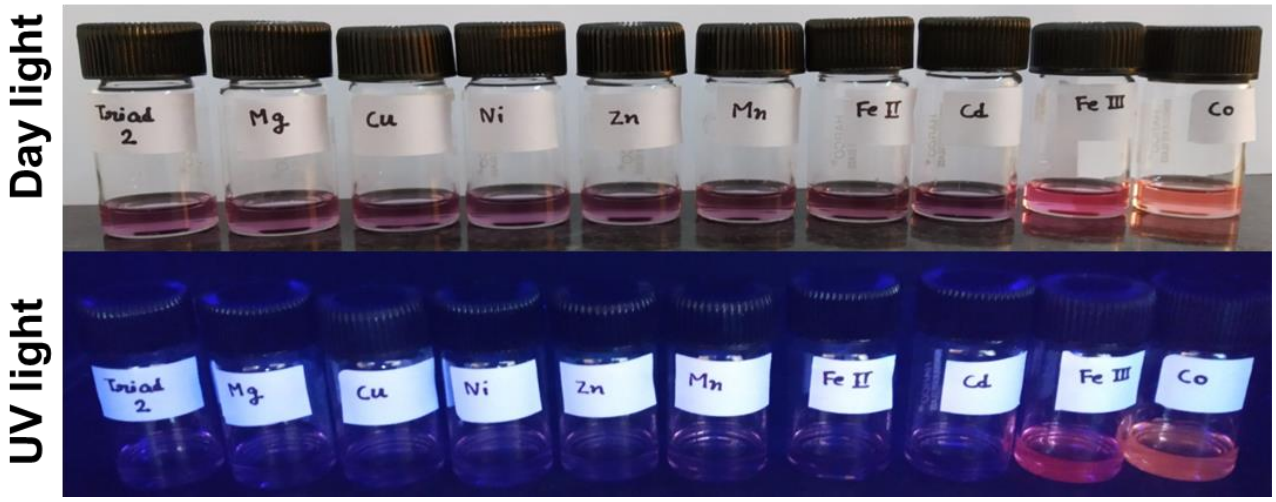

Figure S10. Images of triad **2** with addition of different cations under normal light (top) and under UV light (bottom).

Using the fluorescence titration data[S13], the intensities of the aza-BODIPY fluorescence (I_{725}) were plotted against the mole fraction of the metal cation for both triads **1** and **2** and the Job's plots showed an intersection of the fitted lines of the two sets of data points at a value of 0.67 that revealed a stoichiometry of 1:2 for triads**1** and **2** with Co^{2+}. Similar jobs plots corresponding to intersection of the two intersecting lines were obtained at 0.67 for triads **1** and **2** with Fe^{3+} indicative of a stoichiometry of 1:2 for triads **1** and **2** with Fe^{3+}.

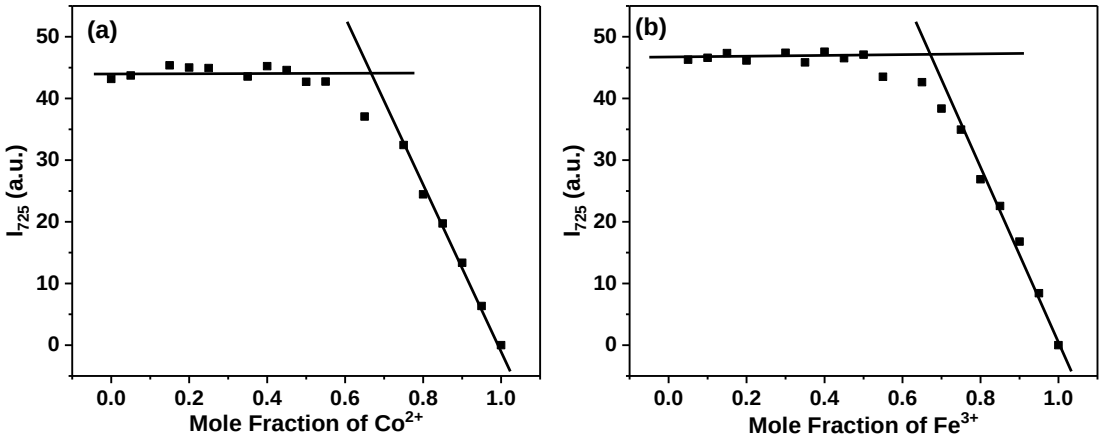

Figure S11. Job's plots for triad **1** with (a) $Co^{2+}$and (b) Fe^{3+}in THF according to aza-BODIPY emission. The total concentration of [Co^{2+}] / [Fe^{3+}] and triad **1** is 10 μM.

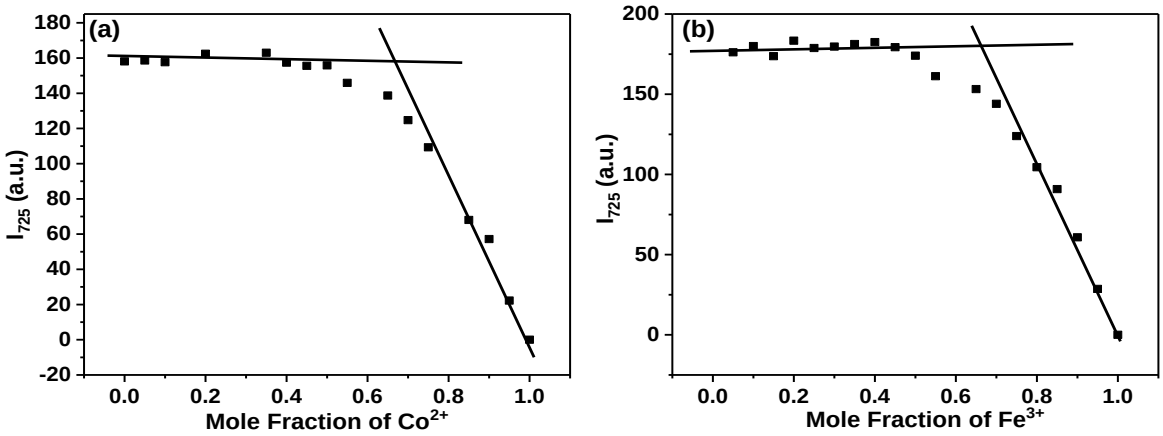

Figure S12. Job's plots for triad **2** with (a) Co^{2+} and (b) Fe^{3+} in THF according to aza-BODIPY emission respectively. The total concentration of [Co^{2+}] / [Fe^{3+}] and triad **2** is 10 μM.

8. Determination of association/binding constants (K_a) for aza-BODIPY using UV/Vis and fluorescence titration

The binding constant of **10** towards Co^{2+} and Fe^{3+} were calculated according to Benesi-Hildebrand equation 6[S14]:

$$\frac{1}{I-I_0} = \frac{1}{\left[K_a (I_{max} - I_0)[G]\right]} + \frac{1}{I_{max} - I_0} \qquad (6)$$

where, I and I_0 are the intensities of fluorescence after addition of metal ions and initial intensity respectively, I_{max} is the maximum intensity upon metal ion addition, [G] is the concentration of the metal ion added (guest) and K_a is the association constant.

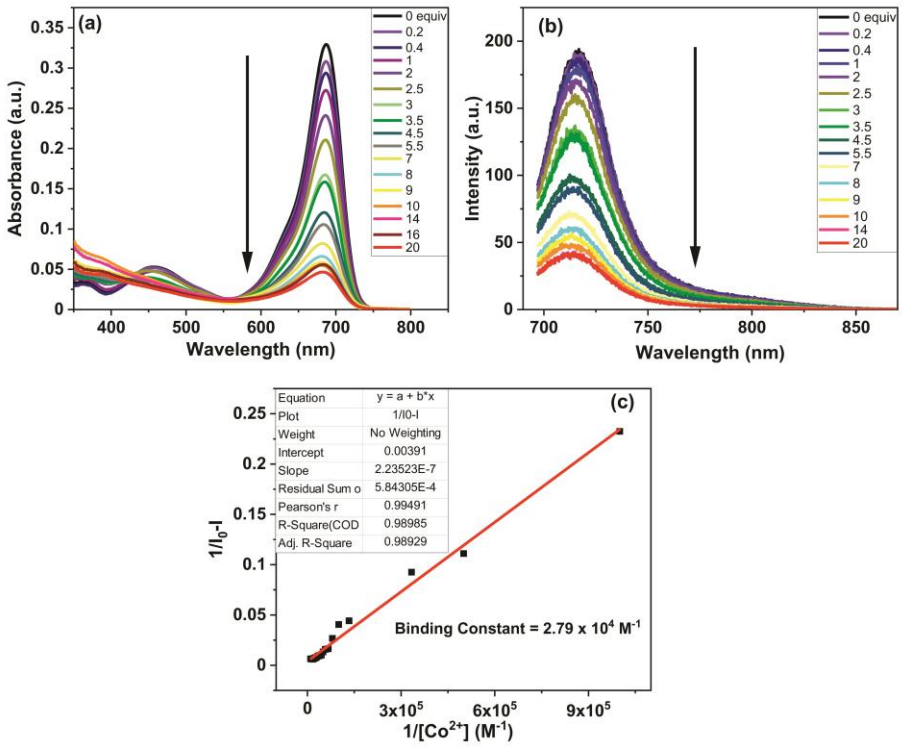

Figure S13. (a) Absorption and (b) fluorescence spectral changes of **10** (5 µM) upon incremental addition of Co^{2+} (0 to 20 equiv.) in THF solution and (c) Benesi-Hildebrand plot of **10**.Co^{2+} association at λ_{em} = 717 nm for calculating binding constant.

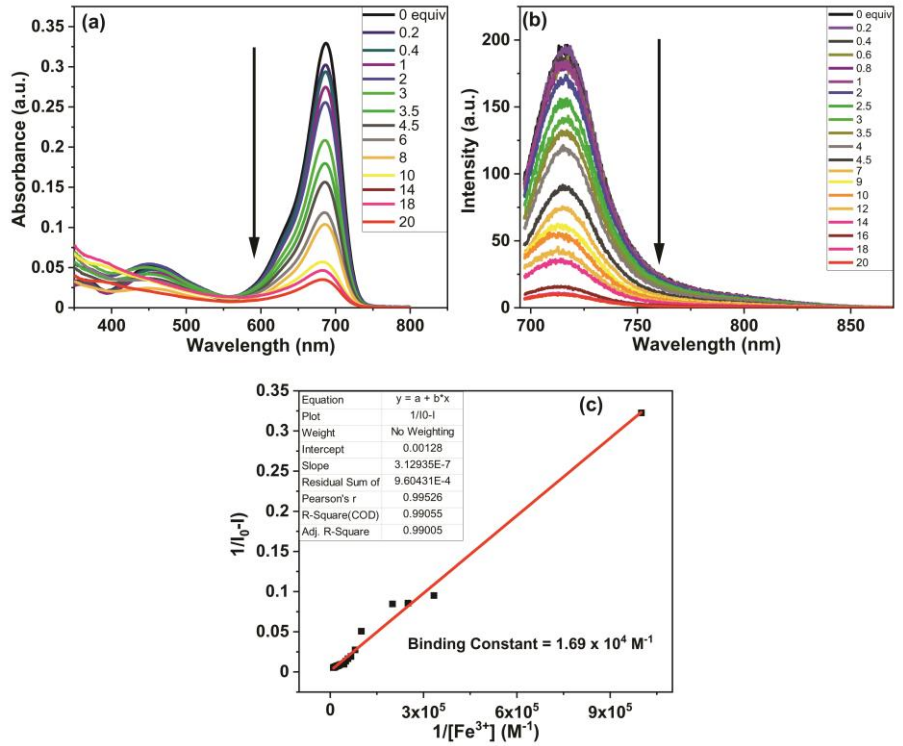

Figure S14. (a) Absorption and (b) fluorescence spectral changes of **10** (5 µM) upon incremental addition of Fe^{3+} (0 to 20 equiv.) in THF solution and (c) Benesi-Hildebrand plot of **10**.Fe^{3+} association at λ_{em} = 717 nm for calculating binding constant.

9. Determination of association/binding constants (K_a) for triads 1 and 2 using UV/Vis and fluorescence titration

The fluorescence titration data of triad **1** with Cu^{2+} and Fe^{3+} and triad **2** with Cu^{2+} and Fe^{3+}did not provide linear data points when Benesi-Hildebrand, Scatchard or Connor models were used.[S14,S15]As a result, two new models that incorporate the ratiometric intensity variation have been used to analyze and fit the fluorescence titration data.[S15,S16] Different analytical approaches are used to determine the stability constants, however, these models have several limitations when applied to ratiometric FRET systems like in the present case. In ratiometric systems, the dynamic range is largely varying i.e., intensities of two bands keep changing constantly during the course of the titration experiment and thus a proper model needs to be utilized for the analysis of the data and for the determination of dissociation/association constants. In this regard, Krężel and co-workers introduced a model where the intensity ratio is calibrated for borderline values of intensities of both wavelengths.[S16] Furthermore, their model takes into account the cooperativity factor, fluorescence artifacts and they have demonstrated the model can be applied to various stoichiometries and experimental conditions and can be used to calculate the dissociation constants (K_d).[S16]

In the present FRET sensors, there are two emission bands arising due to donor emission (λ_1) and acceptor emission (λ_2). Krężel model requires the concentration of unbound ligand (guest) to be calculated and plotted against the ratio of donor (λ_1) and acceptor intensities (λ_2), termed as $R_{1/2}$ or ratio of acceptor to donor intensity $R_{2/1}$. The unbound ligand (here metal) concentration $[L]_u$ can be obtained by first calculating the concentration of host-guest [HG] according the following the seminal review of Thordarson as per the equation 7[S15]:

$$\Delta Y = Y_{\Delta HG}\,([HG]/[H]_0) \qquad (7)$$

where $\Delta Y = Y\text{-}Y_H$, here Y is the experimental parameter under observation, change in fluorescence intensity in present case. Y is the florescence intensity after each addition of metal (I) while Y_H is the initial fluorescence intensity of the host (I_0). $Y_{\Delta HG}$ represents the difference of fluorescence intensity upon maximum addition of guest (I_{max}) and initial fluorescence intensity of host (I_0). [HG] and $[H]_0$ represent the concentration of host-guest complex and the host respectively. Accordingly, the concentration of host-guest complex can be calculated as below:

$$[HG] = (I\text{-}I_0/\ I_{max}\text{-}I_0\ )[H]_0 \qquad (8)$$

Once the [HG] is calculated, the concentration of unbound ligand $[L_u]$ can be calculated by difference of concentration of initial added guest [L] and host-guest complex [HG] as follows:

$$[L_u] = [L]-[HG] \qquad (9)$$

Subsequently, normalized $R_{1/2}$ or normalized $R_{2/1}$ were plotted against $[L_u]$ and data points were fitted with the Krężel model. For ratiometric sensor systems, Krężel model is represented by the following equation[S16]:

$$R_{1/2} = \frac{I_{1b}x^n + I_{1u}K_d^n}{I_{2b}x^n + I_{2u}K_d^n} \qquad (10)$$

$$R_{2/1} = \frac{I_{2b}x^n + I_{2u}K_d^n}{I_{1b}x^n + I_{1u}K_d^n} \qquad (11)$$

where I_{1b} is the intensity at λ_1 of the bound sensor, I_{1u} is the intensity at λ_1 of the unbound sensor, I_{2b} is the intensity at λ_2 of the bound sensor, I_{2u} is the intensity at λ_2 of the unbound sensor, x is the concentration of unbound ligand, K_d is the dissociation constant, and n is Hill's coefficient. Fluorescence titration of triad **1**+Co^{2+} is shown in Figure S15 with indication of the isosbestic point at 699 nm. For FRET sensor triad **1**+Co^{2+}, using the above model gave both the fits ($R_{1/2}$ vs $[L_u]$ and $R_{2/1}$ vs $[L_u]$ give the same result of dissociation constant K_d value (Figure S15).

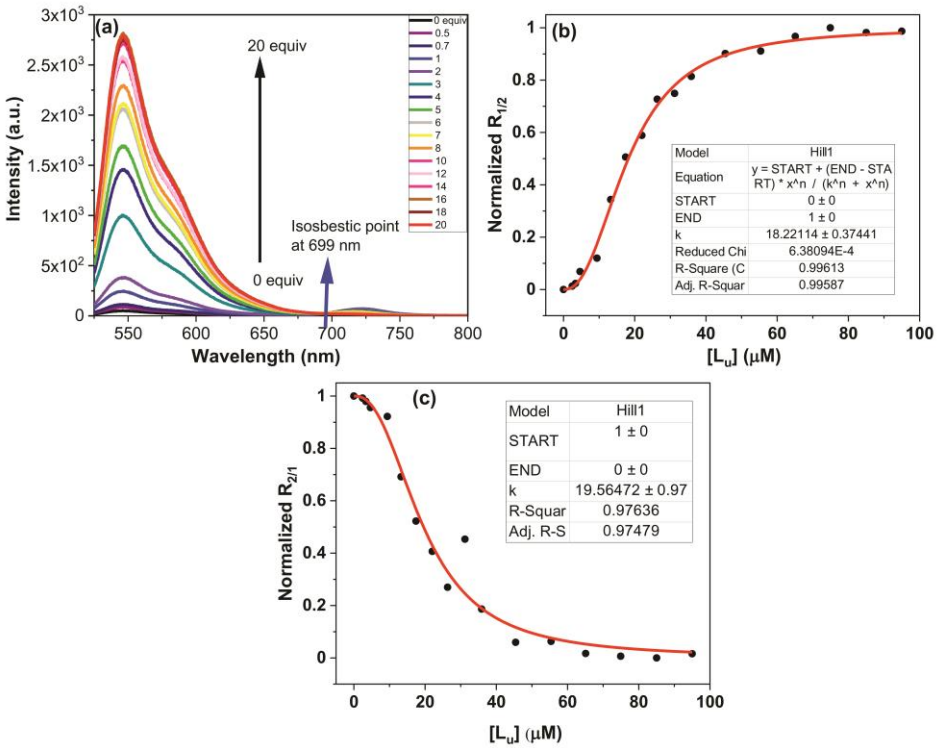

Figure S15. (a) Fluorescence titration of **triad 1** with addition of Co^{2+} and indication of isosbestic point at 699 nm, b) Normalized $R_{1/2}$ plot with concentration of unbound guest, c) Normalized $R_{1/2}$ plot with concentration of unbound guest using Krężel model for determination of association constant.

However for the other three FRET sensor systems (**triad 1**+ Fe^{3+}, **triad 2** + Co^{2+} and **triad 2**+ Fe^{3+}), Krężel model gave different results in the two different fits ($R_{1/2}$ vs $[L_u]$ or $R_{2/1}$ vs $[L_u]$ and this discrepancy is well documented in literature when the donor and acceptor intensity changes might be dissimilar and have been corrected by Merkx using a modified model by taking into account the fluorescence intensity of the isosbestic point.[S17] Dividing either the acceptor or donor intensity by the intensity at the isosbestic wavelength (where intensity is same for donor and acceptor) provides a simple method to avoid the bias that is introduced by plotting acceptor/donor ratios. The approach can be used for the correct determination of equilibrium constants from titration data. The method does not require any additional measurements and could even be applied to more accurately determine K_d values. Utilizing the isosbestic point is like an internal calibration and the K_d values obtained are in between $R_{1/2}$ and $R_{2/1}$ and are more realistic and values obtained from both the $R_{donor/isosbestic}$ or $R_{acceptor/isosbestic}$ are similar,[S17] their average is therefore taken as the K_d value of the system. In the case of three FRET sensor systems (**triad 1**+ Fe^{3+}, **triad 2** + Co^{2+} and **triad 2**+ Fe^{3+}), we have used the fluorescence titration data to fit them to both the Krężel model and the Merkx model and we obtain uniform K_d values using Merkx model in all three cases (presented in Figures S16, S17, S18 and Table S6). The average of the two K_d values (obtained from $R_{Donor/Isosbestic}$vs $[L_u]$ and from $R_{Acceptor/Isosbestic}$ vs $[L_u]$) in Merkx model has been reported as the final K_d values and K_a values have been obtained accordingly (Table S6).

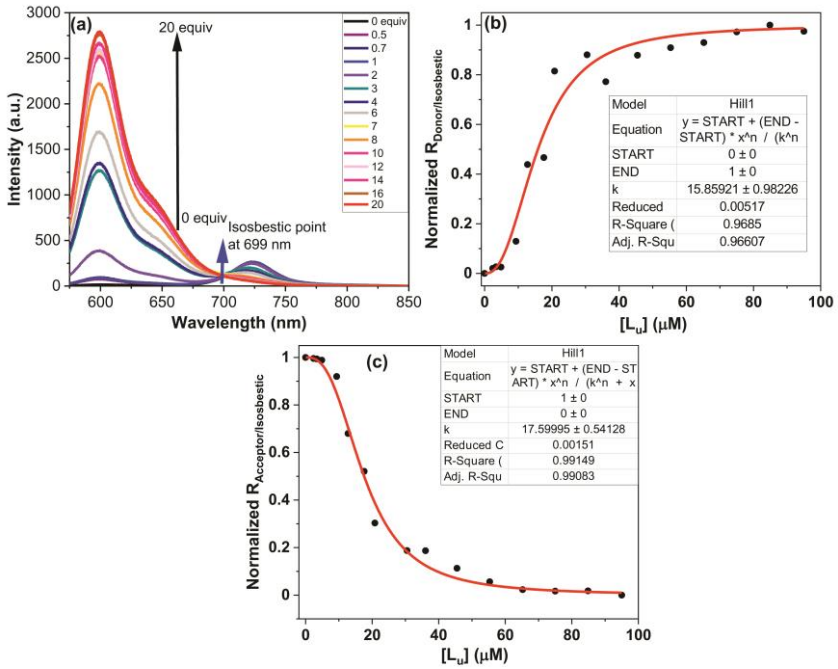

Figure S16. (a) Fluorescence titration of **triad 2** with addition of Co^{2+} and indication of isosbestic point at 699 nm, b) Normalized $R_{donor/isosbestic}$plot with concentration of unbound guest, c) Normalized $R_{acceptor/isosbestic}$plot with concentration of unbound guest using Merkx model for determination of association constant.

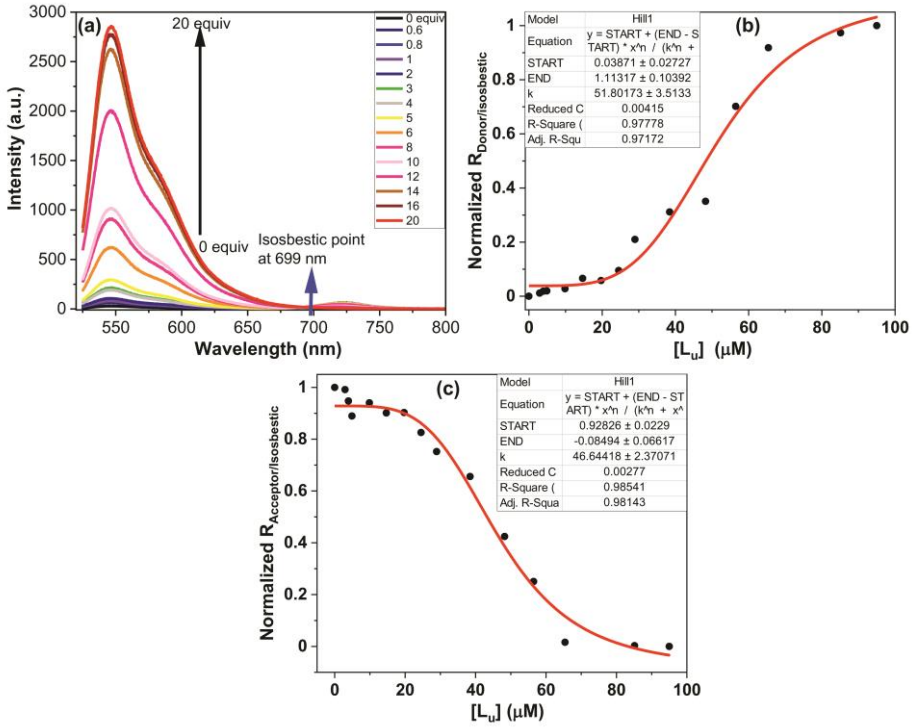

Figure S17. (a) Fluorescence titration of **triad 1** with addition of Fe^{3+} and indication of isosbestic point at 699 nm, b) Normalized $R_{donor/isosbestic}$plot with concentration of unbound guest, c) Normalized $R_{acceptor/isosbestic}$plot with concentration of unbound guest using Merkx model for determination of association constant.

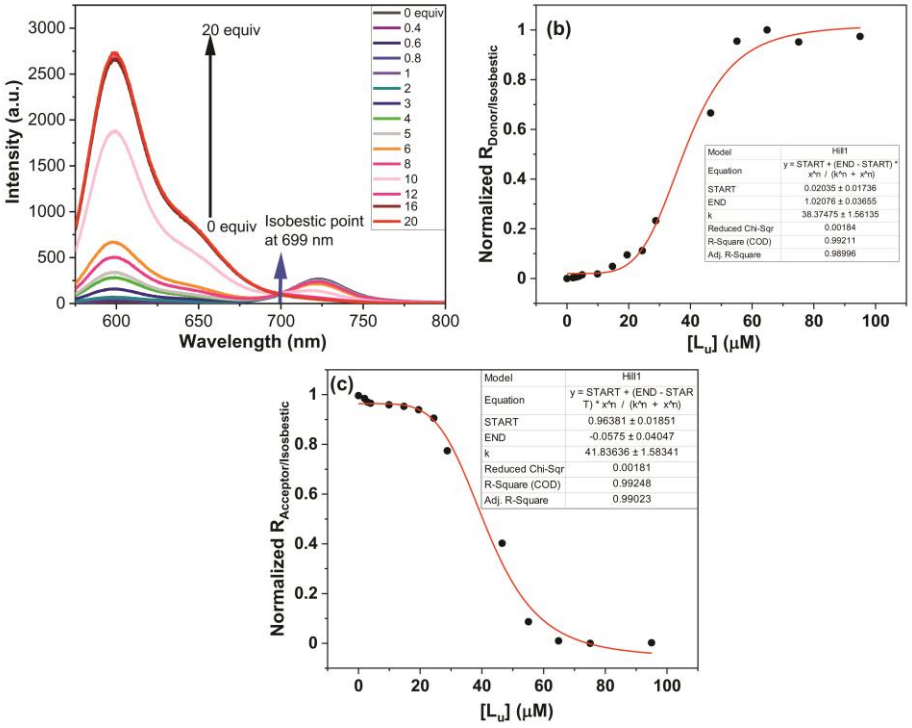

Figure S18. (a) Fluorescence titration of **triad 2** with addition of Fe^{3+} and indication of isosbestic point at 699 nm, b) Normalized $R_{donor/isosbestic}$ plot with concentration of unbound guest, c) Normalized $R_{acceptor/isosbestic}$ plot with concentration of unbound guest using Merkx model for determination of association constant.

Table S6. Calculation of K_d and K_a using two different fitting models (Krężel model and Merkx model) using fluorescence titrations of FRET sensors triads **1** and **2** with Co^{2+} and Fe^{3+}.

FRET Sensor + Guest system	**Fitting Method and model**	**K_d(μM)**	**R^2**	**Average K_d(M)**	**K_a(M^{-1})**
Triad 1 + Co^{2+}	**Krężel model**[S16]				
	$R_{1/2}$ vs unbound guest [L_u] plot	18.2	0.99	**18.85×10^{-6}**	**5.3×10^4**
	$R_{2/1}$vs [L_u]	19.5	0.97		
Triad 2 + Co^{2+}	**Merkx model**[S17]				
	$R_{Donor/Isosbestic}$ vs [L_u]	15.8	0.97		
	$R_{Acceptor/Isosbestic}$ vs [L_u]	17.5	0.99	**16.65×10^{-6}**	**6×10^4**
Triad 1 + Fe^{3+}	**Merkx model**				
	$R_{Donor/Isosbestic}$ vs [L_u]	51.8	0.97		
	$R_{Acceptor/Isosbestic}$ vs [L_u]	46.6	0.98	**49.2×10^{-6}**	**2.03×10^4**
Triad 2 + Fe^{3+}	**Merkx model**				
	$R_{Donor/Isosbestic}$ vs [L_u]	38.4	0.99		
	$R_{Acceptor/Isosbestic}$ vs [L_u]	41.8	0.99	**40.1×10^{-6}**	**2.50×10^4**

10. Thermodynamics of electron transfer upon metal addition in aza-BODIPY and triads

In order to understand the interaction of metal ions with aza-BODIPY **10** as well as triads **1** and **2**, it was important to assess the thermodynamic driving force of electron transfer upon metal addition to the aza-BODIPY and the triads. As UV/Vis absorption studies revealed depletion of absorption of aza-BODIPY upon metal addition that was envisaged as electron transfer from/to metal to/from aza-BODIPY, we started the analysis with aza-BODIPY. Cyclic voltammetry was recorded for aza-BODIPY **10** without and with addition of metal ions (Co^{2+} and Fe^{3+}) along with supporting electrolyte TBAHFP. A shift in the reduction potential of aza-BODIPY upon addition of metal was modelled according to the Nernst equation to obtain the binding constant of the metal with aza-BODIPY according to the following equation and analysis[S18]:

$$E_{red} = E_{red}^0 + (2.3RT/F) \log\{(1 + K_{red}[M^{n+}])/(1 + K_{ox}[M^{n+}])\} \quad (12)$$

where, E_{red}^0 is the one-electron reduction potential in the absence of metal ion, E_{red} is the potential shift in the presence of M^{n+}, K_{red} is the formation constant of the compound$^{-\cdot}$/M^{n+}complex, and K_{ox} is the formation constant of the compound/M^{n+} complex. Because $K_{red}[M^{n+}] >> 1$, and $K_{ox}[M^{n+}] << 1$, above written can be rewritten as follows:

$$\Delta E_{red} = (2.3RT/F) \log K_{red}[M^{n+}]$$

Accordingly, utilizing the value of K_{red}, the driving force for electron transfer in presence of metal ion ($-\Delta G_{ET}$) can be calculated according to the following equation:

$$-\Delta G_{ET} = -\Delta G_{ET}^{0} + RT \ln(K_{red}[M^{n+}]) \quad (13)$$

where, $-\Delta G_{ET}^{0}$ is the driving force of electron transfer in a donor-acceptor system and K_{red} is the binding constant as calculated above.

Furthermore, the K_{red} values correspond to free energy changes for metal ion binding and a negative free energy change in indicative of the spontaneity of the binding event, the binding free energy change can be calculated according to the following equation[S18]:

$$\text{Binding free energy changes} = -RT \ln K_{red} \quad (14)$$

In order to calculate the thermodynamic parameters for the electron transfer process in presence of metal ions (Co^{2+} and Fe^{3+}), CV measurements were performed for compound **10** in presence of the supporting electrolyte TBAHFP and by adding 20 equiv. of Co^{2+} and Fe^{3+} in THF. The solvent used for CV measurement was THF because both the compound (**10**, triads **1** and **2**) and the metal perchlorate salts were soluble in THF. Figure S19 show the cyclic voltammograms of compounds **10**without and with Co^{2+} and Fe^{3+}. Based on the shift of the reduction potential observed in case of **10**+Co^{2+} compared to the first reduction potential of **10** in THF, the K_{red} and the ΔG_{ET} (-0.165 eV) was calculated according to the analysis discussed earlier (analysis of Fukuzumi[S18]) as presented in Table S7. Furthermore, the binding free energy change for **10** + Co^{2+} according to equation 14 was -0.259 eV. The cyclic voltammogram of **10** + Fe^{3+} also showed a shift in the reduction side. Usually, both the +2 and +3 oxidation states of Fe are stable and there could be scrambling of the two oxidation states in the presence of aza-BODIPY compound **10** under CV measurement conditions. Presumably due to presence of small amount of Fe^{2+} which in the process of getting oxidized to Fe^{3+} can reduce aza-BODIPY to aza-BODIPY$^{\cdot-}$ and so a shift in the reduction potential of aza-BODIPY can be expected. Following the Fukuzumi analysis (eq.s 12-14) as above, ΔG_{ET} (-0.135 eV) and binding free energy change for **10** + Fe^{3+} was calculated as -0.23 eV. Thus, the values of ΔG_{ET} and binding free energy terms for compound **10** in presence of either Co^{2+} or Fe^{3+} indicate the spontaneity of electron transfer in case of **10** in the presence of Co^{2+} and Fe^{3+}.

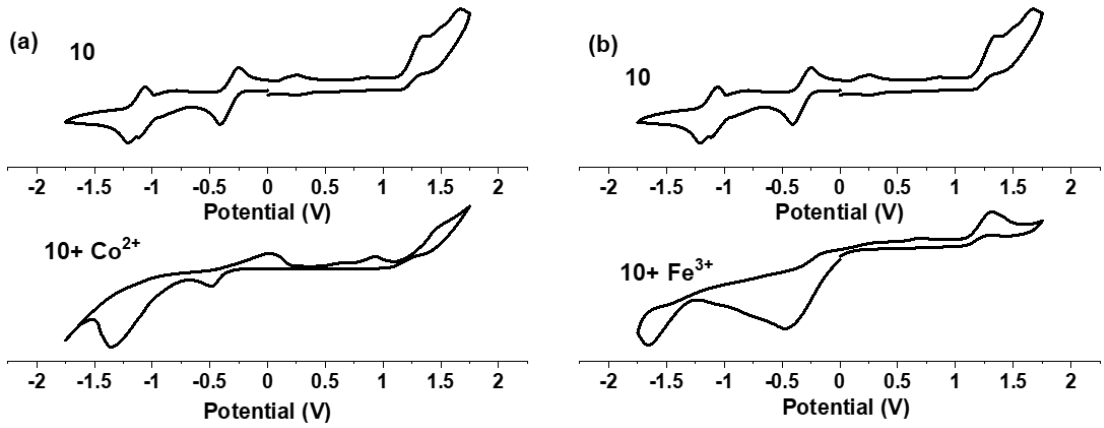

Figure S19. Cyclic voltammogram of (a)**10, 10 + Co^{2+}** and (b) **10, 10 + Fe^{3+}** in dry THF with 0.1 M tetrabutylammonium hexafluorophosphate ($TBAHPF_6$) vs Ag/AgCl reference electrode at scan rate of 0.1 V/s (**10**; $c \sim 1.28$ mM and Co^{2+} / Fe^{3+}; $c \sim 25$ mM).

Table S7. Thermodynamic parameters (ΔG_{ET}) of electron transfer upon addition of metal ions in compounds using cyclic voltammetry in deaerated THF at 298 K.

Compounds with/without M^{n+}	Relevant CV peaks showing shift	K_{red} (M^{-1})	ΔG_{ET} (eV)	Binding free energy change (eV)
	First Reduction (V)			
10	-0.32	-	-	-
10+ Co^{2+}	-0.49	2.4×10^4	-0.165	-0.259
10 + Fe^{3+}	-0.46	7.7×10^3	-0.135	-0.230

Followed by the thermodynamic analysis for electron transfer in case of **10** in presence of metal ions, CV measurements were performed for triad **2** in THF in absence of metal ions and then after addition of Co^{2+} and Fe^{3+} (Figure S20). The analysis of ΔG_{ET} in this case was complicated because of the fact that triad **2** has two redox active moieties PDI and aza-BODIPY and several peaks in the reduction side (two reductions of PDI and aza-BODIPY each) also evident from its CV recorded in DCM shown in manuscript figure 6d. Moreover, the solubility of the triad **2** in THF was not appreciable like in DCM and as a result the current obtained and clarity of peaks in CV was not very high. Some of these peaks were partially overlapped in THF. Upon addition of metal ions (Co^{2+} and Fe^{3+}), the CV of triad **2 c**hanged significantly in the reduction side however, it was not possible to ascertain from the cyclic voltammograms which peak corresponded to the first reduction of aza-BODIPY due to significant overlap and flattening of the peaks. Therefore, the lack of discernible peaks in CV precluded the calculation of ΔG_{ET} for triad **2** as per the analysis performed earlier form the aza-BODIPY compound **10** in presence of metal ions.

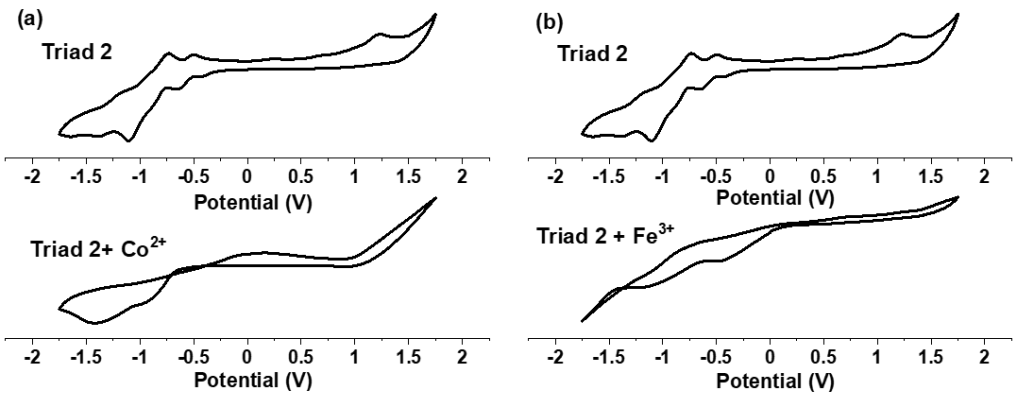

Figure S20. Cyclic voltammogram of (a)Triad **2,** Triad **2 + Co^{2+}** and (b) Triad **2,** Triad **2 + Fe^{3+}** in dry THF with 0.1 M tetrabutylammonium hexafluorophosphate ($TBAHPF_6$) vs Ag/AgCl reference electrode at scan rate of 0.1 V/s (Triad **2**; *c* ~ 1 mM and Co^{2+}/Fe^{3+}; *c* ~ 20 mM).

Nevertheless, we used other several supporting evidences as discussed below to assess the possibility of electron transfer in case of triads **1** and **2** in presence of metal ions. Firstly, in aza-BODIPY **10**, the electron transfer from/to Co^{2+}/Fe^{3+} is spontaneous as shown above (Table S7). From UV/Vis measurements, it was observed that absorption of aza-BODIPY got depleted upon metal addition (Co^{2+} or Fe^{3+}) and spectroelectrochemical measurements discussed next section indicate the formation of radical anion/cation of aza-BODIPY characterized by depleted absorption bands. Therefore, electron transfer from/to metal ions and formation of radical anion/cation of aza-BODIPY is the most likely reason for depletion of its absorption. Furthermore, UV/Vis studies of triads **1** and **2** in presence of metal ions showed that it is only the aza-BODIPY absorption that is depleted upon addition of metal ions and no change in PDI absorption occurred in triads **1** and **2** (Figures 11a,c, 12a,c). Thus, it is reasonable to propose that the aza-BODIPY shows similar redox behaviour (i.e., it gets transformed into radical anion/cation in presence of metals) in case of triads upon metal addition (Co^{2+}, Fe^{3+}) like it behaves independently in presence of metal ions.

11. Spectroelectrochemistry

During the oxidation cycle, Aza-BODIPY[S19,S20] **10** shows a gradual depletion of the absorption band at 682 nm and a concomitant appearance of new shoulder band at 751 nm. During the reduction cycle, aza-BODIPY shows a rapid depletion of the absorption band at 682 nm and a mild band appearing at 825 nm. Energy donor subchromophores PDI[S21] **3** and PDI **4** showed typical bands of radical anion and dianion formation upon the reduction cycles while they were mostly non-responsive in the oxidation cycle. PDI **4** showed formation of three new NIR bands at 691 nm, 781 nm and 974 nm and depletion of the main PDI absorption band at 575 nm while PDI **3** showed formation of three new NIR bands at 675 nm, 756 nm and 920 nm and depletion of the main PDI

absorption band at 520 nm. PDI **3** and **4** was non responsive to the oxidation cycle and barely showed any change in the spectroelectrochemical features during the oxidation cycle.

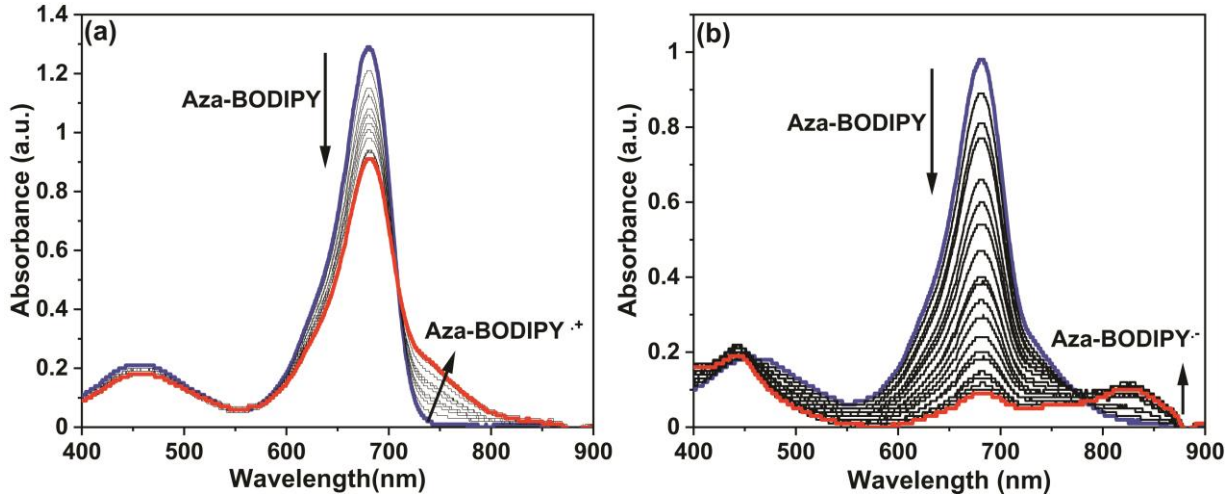

Figure S21. Spectroelectrochemical changes observed in for aza-BODIPY **10** during a) oxidation b) reduction cycle.

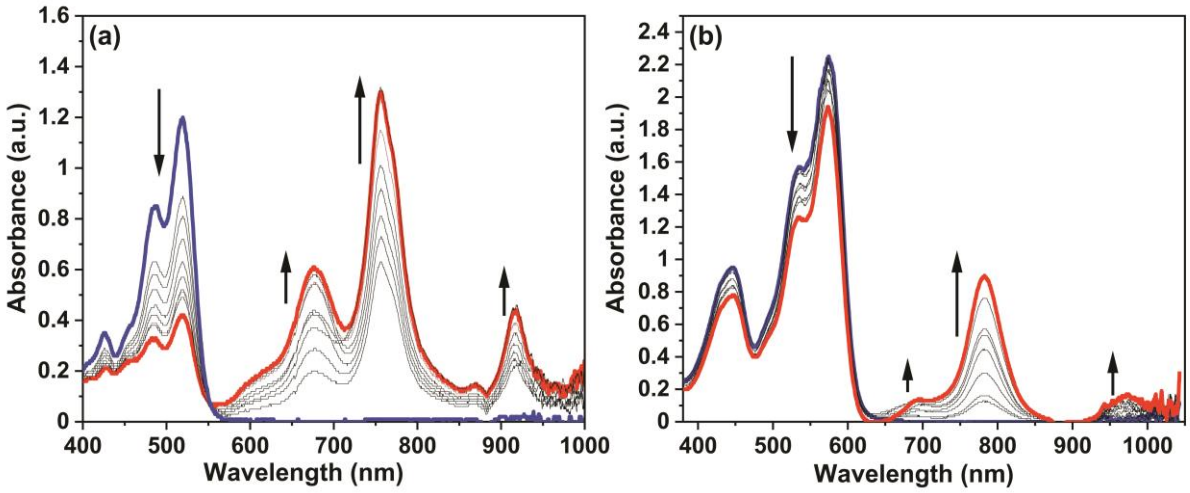

Figure S22. Spectroelectrochemical changes observed in for a) PDI **3** and b) PDI **4** during reduction cycle.

12. Control experiment with TEMPO

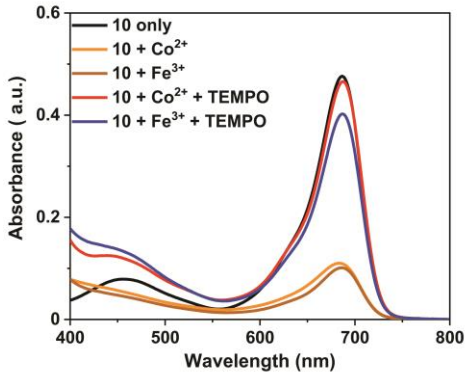

Figure S23. Absorption spectral changes of **10** (c ~ 5 µM) **(**upon addition of metal ions (~20 equiv.) and metal ion (~20 equiv.) + TEMPO (~30 equiv.).

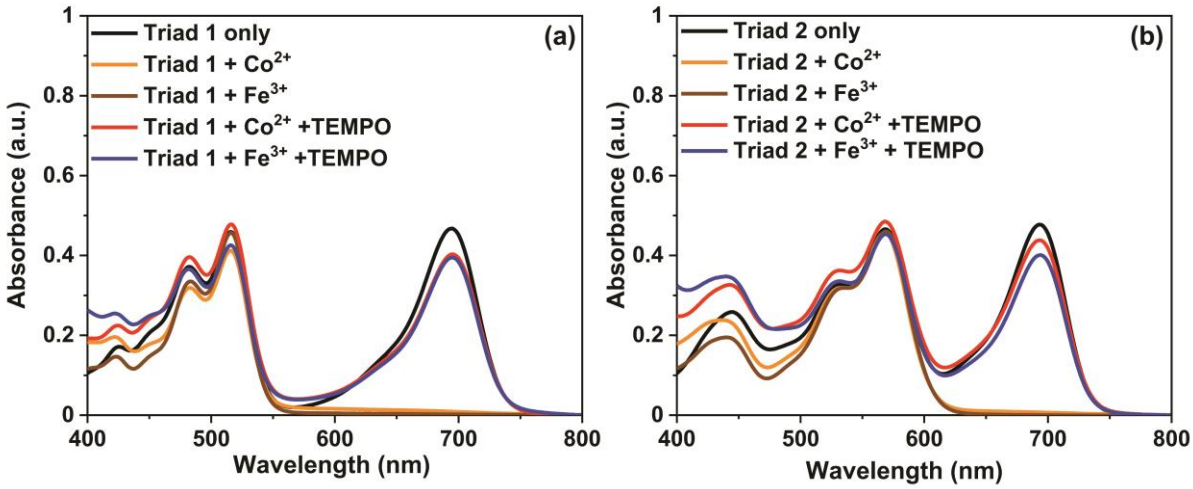

Figure S24. Absorption spectral changes of (a) triad **1** (c ~ 5 µM) and (b) triad **2** (c ~ 5 µM) upon addition of metal ions (20 equiv.) and metal ion (~20 equiv.) + TEMPO (~30 equiv.).

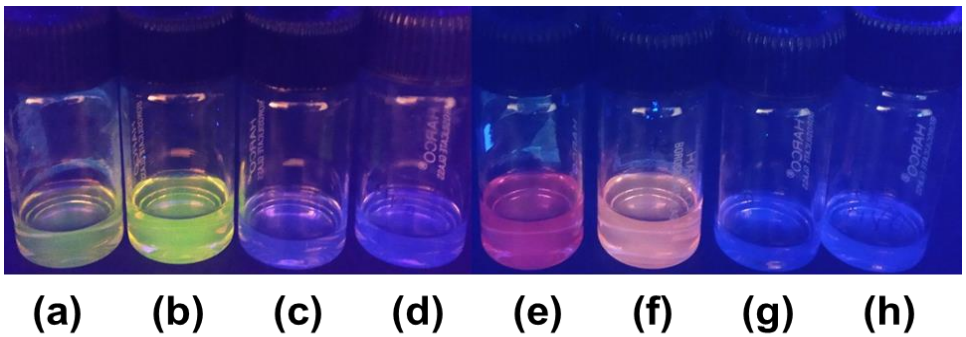

Figure S25. Photographs taken under UV light of (a) triad **1** + Co^{2+} (b) triad **1** + Fe^{3+} (c) triad **1** + Co^{2+} + TEMPO (d) triad **1** +Fe^{3+}+ TEMPO (e) triad **2** + Co^{2+} (f) triad **2** + Fe^{3+} (g) triad **2** + Co^{2+} + TEMPO (h) triad **2** + Fe^{3+} + TEMPO under UV light . (Triad **1**/**2**; *c* ~ 5 µM, Co^{2+}/ Fe^{3+}~ 20 equiv. and TEMPO ~ 30 equiv.). The solutions of triads without TEMPO showed fluorescence (a, b, e, f) due to the PDI units and indicative of FRET turn off while the solutions with TEMPO do not show any fluorescence indicative of the quenching of the radical anion/cation species by TEMPO formed in presence of metal ions and efficient FRET from PDI to aza-BODIPY.

13. DFT Calculations

Figure S26 represents the frontier molecular orbitals of triads **1** and **2** as obtained by density functional theory (DFT) calculations at B3LYP 6-31G (d,p) level.[S1] For triads **1** and **2**, the highest occupied molecular orbital (HOMO) was located on the aza-BODIPY while lowest unoccupied molecular orbital (LUMO) was located on the PDI unit. The centre-to-centre distance between PDI unit and aza-BODIPY unit for triads **1** and **2** were found to be 18.96 Å and 18.68 Å respectively from the geometry optimizations. Table S8 shows the calculated FMO energy levels for triads **1** and **2** and table S9 shows the first three frequencies obtained from frequency calculations for triads **1** and **2**.

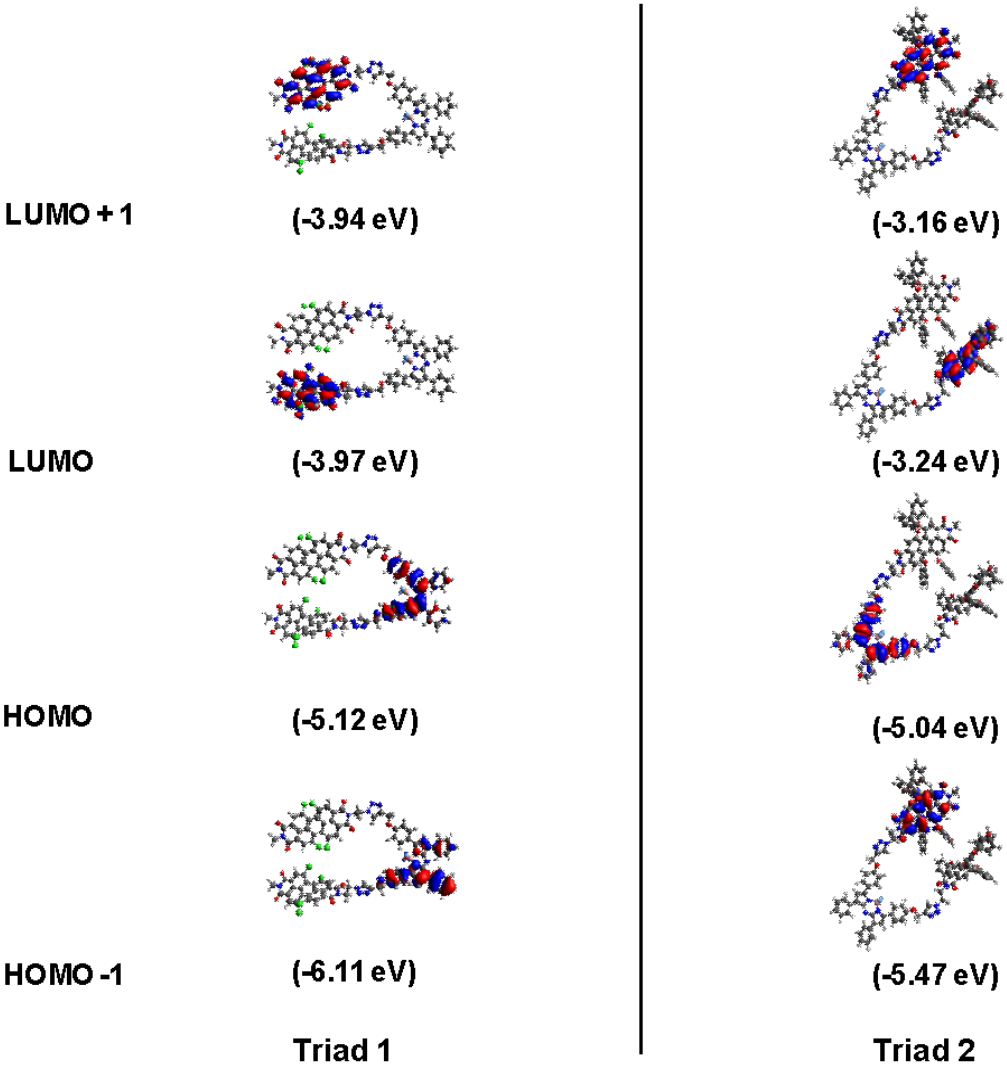

Figure S26. Frontier Molecular Orbitals of triad **1** and **2** as obtained by DFT method at B3LYP 6-31G (d,p) level.

Table S8. FMO energy levels calculated using B3LYP/6-31G (d,p) calculations.

Compound	HOMO-1 (eV)	HOMO (eV)	LUMO (eV)	LUMO+1 (eV)	E_g (eV)
Triad **1**	-6.11	-5.12	-3.97	-3.94	1.15
Triad **2**	-5.47	-5.04	-3.24	-3.16	1.80

Table S9. First three frequencies obtained from frequency calculations for triads **1** and **2**.

Compound	First three frequencies
Triad **1**	1.52 2.28 3.31
Triad **2**	2.28 2.69 3.21

Coordinates of geometry optimized structure of triad 1

N	-13.15462	-1.53009	0.81428
C	-12.30599	-2.40980	0.30986
N	-10.95149	-2.15216	0.09051
B	-10.28154	-0.78984	0.48569
N	-11.45456	0.16303	0.90633
C	-12.75666	-0.30115	1.09710
C	-12.61650	-3.73949	-0.14820
C	-11.42362	-4.23825	-0.65278
C	-10.41093	-3.25605	-0.49950
C	-13.59547	0.79452	1.50833
C	-12.76576	1.90717	1.51555
C	-11.45324	1.50380	1.15518
H	-11.26435	-5.21356	-1.08778
H	-13.03084	2.90710	1.82539
C	-13.90838	-4.43091	-0.08762
C	-15.02235	0.74605	1.83630
C	-16.36011	-5.81997	-0.02274
C	-15.15443	-6.52484	-0.03470
C	-13.94406	-5.83897	-0.06641

C	-16.34052	-4.42426	-0.04002
C	-15.13150	-3.73294	-0.07257
H	-17.30532	-6.35433	0.00147
H	-15.15690	-7.61075	-0.01219
H	-15.12398	-2.65052	-0.08826
H	-17.27294	-3.86714	-0.03444
H	-13.01257	-6.39618	-0.04914
C	-15.63401	-0.42607	2.32138
C	-16.98836	-0.43510	2.64734
H	-15.03977	-1.32324	2.44205
C	-17.76005	0.71915	2.50141
C	-17.16621	1.88868	2.02117
C	-15.81419	1.90174	1.69210
H	-18.81511	0.70828	2.75874
H	-17.44068	-1.34757	3.02485
H	-15.36677	2.80813	1.29600
H	-17.75927	2.79001	1.89649
C	-9.02208	-3.42961	-0.92538
C	-10.30241	2.40273	1.08491
C	-8.75794	-4.24329	-2.04188
C	-7.92050	-2.86508	-0.24700
C	-7.46067	-4.48429	-2.48493
C	-6.62621	-3.10792	-0.67417
C	-6.38243	-3.91508	-1.79553
C	-8.98437	2.00839	1.40102
C	-10.51822	3.74616	0.72817
C	-7.94280	2.91807	1.34905
C	-8.17464	4.25068	0.97578
C	-9.47569	4.66634	0.66577

H	-7.30583	-5.10087	-3.36173
H	-9.58486	-4.67185	-2.59860
H	-5.77804	-2.68324	-0.14774
H	-8.08697	-2.25376	0.62953
H	-11.51790	4.07401	0.46233
H	-6.93034	2.61974	1.59955
H	-8.78828	0.99027	1.70866
H	-9.68509	5.68787	0.37289
O	-5.07281	-4.08408	-2.13249
O	-7.07690	5.05628	0.94993
C	-4.75942	-4.90337	-3.25543
C	-3.27098	-4.93992	-3.39083
H	-5.20877	-4.49924	-4.17237
H	-5.15871	-5.91726	-3.10899
C	-7.22945	6.41546	0.54829
C	-5.86719	7.03143	0.54014
H	-7.88615	6.95880	1.24079
H	-7.68397	6.46657	-0.45143
C	-2.29080	-4.50354	-2.52861
C	-4.63224	6.42826	0.61146
N	-2.67457	-5.47008	-4.49717
N	-1.37870	-5.38668	-4.36566
N	-1.13000	-4.79381	-3.17589
H	-2.32765	-4.02212	-1.56513
N	-5.68958	8.38029	0.44071
N	-4.41078	8.64437	0.44434
N	-3.75588	7.46629	0.55586
H	-4.32455	5.39960	0.70481
C	-2.30316	7.42286	0.53458

C	-1.77640	7.15358	-0.88642
H	-1.97569	6.63062	1.21111
H	-1.94539	8.38539	0.90409
N	-0.34481	6.82272	-0.87177
H	-1.90820	8.03400	-1.51322
H	-2.30565	6.30287	-1.31705
C	-0.00640	5.49557	-0.57047
C	0.57904	7.83416	-1.19169
C	1.43583	5.15592	-0.58291
C	2.01118	7.44430	-1.18453
C	2.41780	6.15193	-0.78255
O	-0.87447	4.67281	-0.31136
O	0.20823	8.96554	-1.46076
C	1.81798	3.83249	-0.53844
C	3.17854	3.49487	-0.56683
C	4.19161	4.46540	-0.42471
C	3.80208	5.82723	-0.68875
C	4.78727	6.81730	-1.04381
C	4.30261	7.94587	-1.73697
C	2.94687	8.30670	-1.71388
Cl	3.50964	1.82958	-0.99526
H	1.06034	3.05801	-0.53840
Cl	5.28529	8.87403	-2.84809
H	2.62048	9.23746	-2.16242
C	0.73117	-5.83171	-1.92780
C	0.24159	-4.61263	-2.72725
F	-9.57100	-0.26475	-0.57063
F	-9.45528	-1.00264	1.60564
H	0.85629	-4.47423	-3.61848

N	2.08819	-5.61860	-1.40440
H	0.75735	-6.70867	-2.57295
H	0.07306	-6.00750	-1.07648
C	2.20295	-4.91764	-0.19301
C	3.57386	-4.73282	0.34081
C	3.16825	-6.09811	-2.17021
C	4.52035	-5.92149	-1.58627
O	2.98165	-6.63097	-3.25262
O	1.20823	-4.49001	0.37656
C	4.69135	-5.24232	-0.35870
C	5.62606	-6.37597	-2.27667
C	6.90648	-6.28756	-1.70262
C	5.99603	-5.06677	0.17361
C	7.10232	-5.76754	-0.41270
C	3.75620	-4.10049	1.55443
C	5.05309	-3.84721	2.03447
C	6.19498	-4.18983	1.29177
Cl	8.23738	-6.74314	-2.73901
H	5.49604	-6.81767	-3.25747
H	2.89122	-3.78703	2.12662
Cl	5.15098	-3.20073	3.65541
C	6.20231	6.51966	-0.81094
C	5.60547	4.16938	-0.18866
C	6.59039	5.15755	-0.54649
C	8.33372	-5.83503	0.38393
C	7.57643	-3.77145	1.56094
C	8.60667	-4.71597	1.23848
C	7.99571	-2.53214	2.07100
C	9.91085	-4.54048	1.77117

C	9.25557	-6.89373	0.41920
C	7.21923	7.48617	-0.66900
C	8.58009	7.14386	-0.69446
C	8.96042	5.82040	-0.65091
C	7.97340	4.82908	-0.45323
C	8.37685	3.53769	-0.04723
C	7.44244	2.67870	0.48874
C	6.08796	3.04310	0.50865
H	9.33952	7.91658	-0.69175
Cl	6.89437	9.15148	-0.24069
H	7.76859	1.74926	0.94054
Cl	5.09845	2.12570	1.62569
C	10.40773	5.47982	-0.65849
N	10.73374	4.14137	-0.39380
C	9.81026	3.14916	-0.04627
C	12.14738	3.74415	-0.40564
O	10.18411	2.02115	0.23871
O	11.26732	6.31757	-0.88532
H	12.73018	4.60235	-0.72969
H	12.28320	2.90239	-1.08660
H	12.45412	3.43077	0.59460
C	10.51513	-6.75758	1.02990
C	10.86766	-5.57221	1.64236
C	10.24582	-3.33428	2.42583
H	11.22443	-7.57622	1.00892
C	9.31447	-2.31965	2.51065
H	9.60502	-1.36485	2.93232
Cl	8.86672	-8.49083	-0.17393
Cl	6.95290	-1.12851	2.08188

C	11.61101	-3.13049	2.97419
C	12.23366	-5.41819	2.20910
N	12.51457	-4.19253	2.83310
C	13.85531	-3.98163	3.39448
H	14.43639	-4.88166	3.21210
H	13.77924	-3.78325	4.46530
H	14.32193	-3.11775	2.91734
O	11.95046	-2.09611	3.52832
O	13.06822	-6.30753	2.13703
H	0.28670	-3.71306	-2.10976

Coordinates of geometry optimized structure of triad 2

N	-14.51022	1.17709	-0.82586
C	-13.74452	2.22707	-0.58234
N	-12.39844	2.14615	-0.22058
B	-11.63328	0.77887	-0.13583
N	-12.72409	-0.33688	-0.29402
C	-14.03201	-0.04811	-0.68450
C	-14.15321	3.60841	-0.58300
C	-13.02733	4.32130	-0.19627
C	-11.95827	3.41337	0.02250
C	-14.78407	-1.27303	-0.76525
C	-13.90000	-2.27096	-0.37852
C	-12.63690	-1.68428	-0.10371
H	-12.94943	5.39200	-0.08057
H	-14.09191	-3.33360	-0.36621
C	-15.46987	4.15475	-0.92788
C	-16.18653	-1.42976	-1.15865
C	-17.97603	5.28015	-1.55864

C	-16.81066	6.03589	-1.70485
C	-15.57340	5.48007	-1.39377
C	-17.88881	3.96411	-1.10133
C	-16.65270	3.40333	-0.78779
H	-18.94221	5.71317	-1.80064
H	-16.86504	7.05794	-2.06849
H	-16.59277	2.38290	-0.43136
H	-18.78968	3.36930	-0.98097
H	-14.67169	6.06766	-1.53569
C	-16.82354	-0.51547	-2.01977
C	-18.15192	-0.70344	-2.39490
H	-16.26908	0.33727	-2.39133
C	-18.87193	-1.80368	-1.92569
C	-18.25249	-2.71836	-1.07091
C	-16.92644	-2.53327	-0.69158
H	-19.90679	-1.94751	-2.22221
H	-18.62400	0.01032	-3.06383
H	-16.46082	-3.23543	-0.00690
H	-18.80584	-3.57349	-0.69371
C	-10.61661	3.80515	0.45275
C	-11.44781	-2.43359	0.29880
C	-10.47750	4.94047	1.27168
C	-9.44113	3.13140	0.05627
C	-9.23170	5.38859	1.70077
C	-8.19733	3.57616	0.46936
C	-8.07858	4.70249	1.29809
C	-10.13506	-2.07340	-0.07520
C	-11.61588	-3.60463	1.05958
C	-9.05414	-2.85171	0.30064

C	-9.23988	-4.01210	1.06790
C	-10.53391	-4.38757	1.45146
H	-9.17341	6.25451	2.34859
H	-11.36377	5.46622	1.61160
H	-7.29229	3.06462	0.15945
H	-9.51032	2.27048	-0.59466
H	-12.61117	-3.89372	1.38126
H	-8.04527	-2.58271	0.00627
H	-9.97295	-1.19243	-0.68145
H	-10.70758	-5.26935	2.05585
O	-6.81011	5.04428	1.65495
O	-8.10795	-4.69835	1.38658
C	-6.61783	6.18308	2.49200
C	-5.14964	6.32508	2.73365
H	-7.14024	6.05988	3.44960
H	-7.02406	7.08075	2.00354
C	-8.22707	-5.90406	2.13938
C	-6.85463	-6.47245	2.30423
H	-8.88292	-6.61177	1.61184
H	-8.66960	-5.71122	3.12535
C	-4.08437	5.76719	2.06328
C	-5.70406	-6.22501	1.58961
N	-4.66887	7.10432	3.74441
N	-3.36354	7.05934	3.73439
N	-2.99471	6.24327	2.72196
H	-4.01971	5.09219	1.22560
N	-6.58345	-7.41123	3.25578
N	-5.32737	-7.75751	3.16849
N	-4.78091	-7.04577	2.15698

H	-5.47926	-5.56173	0.77021
C	-3.36321	-7.16598	1.85250
C	-2.55686	-6.00842	2.46553
H	-3.24148	-7.17016	0.76703
H	-3.03214	-8.12214	2.26074
N	-1.16616	-6.02334	1.99694
H	-2.54444	-6.09469	3.55097
H	-2.99494	-5.05539	2.16724
C	-0.20038	-6.64266	2.81555
C	-0.91345	-5.44231	0.74315
C	1.19946	-6.58160	2.33951
C	0.49206	-5.44098	0.28360
C	1.51074	-5.99615	1.09208
O	-0.52743	-7.18806	3.86019
O	-1.83337	-4.97094	0.08365
C	2.20006	-7.14561	3.10755
C	3.54576	-7.04233	2.71289
C	3.91352	-6.34621	1.54223
C	2.86181	-5.96791	0.64586
C	3.14813	-5.56162	-0.69814
C	2.12841	-4.90126	-1.41073
C	0.80989	-4.85283	-0.92522
H	1.92943	-7.65740	4.02242
H	0.02880	-4.36291	-1.49334
C	-1.04958	7.06057	1.42907
C	-1.58557	6.02463	2.43114
F	-10.97179	0.65648	1.06539
F	-10.74433	0.69325	-1.22420
H	-1.04385	6.09703	3.37566

N	0.32109	6.73697	1.01705
H	-1.03859	8.04802	1.88844
H	-1.67047	7.06460	0.53308
C	1.37824	7.30990	1.75052
C	2.74683	7.00275	1.27984
C	0.47149	5.83537	-0.05067
C	1.85650	5.53383	-0.47218
O	-0.51387	5.33872	-0.58458
O	1.14784	8.02194	2.71835
C	2.95391	6.12330	0.19339
C	2.06821	4.69315	-1.54792
C	3.37408	4.33195	-1.92187
C	4.27964	5.82295	-0.22993
C	4.49510	4.78459	-1.19426
C	3.82751	7.54798	1.94502
C	5.13484	7.32563	1.47809
C	5.37804	6.56481	0.31580
H	1.21086	4.31149	-2.08721
H	3.64799	8.15641	2.82230
C	4.49425	-5.81895	-1.21073
C	5.28704	-6.02510	1.14545
C	5.55943	-5.89972	-0.25652
C	5.86871	4.31046	-1.38003
C	6.67801	6.43233	-0.34498
C	6.93044	5.22142	-1.06738
C	7.68334	7.42123	-0.36326
C	8.25748	4.91878	-1.48257
C	6.23027	3.01357	-1.79716
C	4.81831	-6.03992	-2.56582

C	6.15678	-6.06477	-2.99879
C	7.18844	-5.93242	-2.09092
C	6.90849	-5.86610	-0.70817
C	7.95928	-5.75570	0.22879
C	7.67797	-5.66203	1.57656
C	6.35332	-5.78398	2.03617
H	6.39405	-6.17160	-4.05001
H	8.49351	-5.50159	2.27022
C	8.58725	-5.89168	-2.58562
N	9.58960	-5.75995	-1.61084
C	9.36768	-5.68431	-0.22867
C	10.98892	-5.69392	-2.04745
O	10.31112	-5.56599	0.54165
O	8.86134	-5.96928	-3.77572
H	11.00100	-5.76662	-3.13176
H	11.55490	-6.51361	-1.60016
H	11.43375	-4.75232	-1.71938
C	7.56180	2.69118	-2.11702
C	8.55433	3.64504	-2.01652
C	9.27156	5.89324	-1.35609
H	7.82529	1.69745	-2.45626
C	8.97164	7.14412	-0.85506
H	9.74719	7.89925	-0.83837
C	10.65430	5.59964	-1.80098
C	9.93605	3.29845	-2.43139
N	10.89881	4.31322	-2.30166
C	12.27684	4.03037	-2.71784
H	12.31154	3.00301	-3.07080
H	12.95422	4.17040	-1.87298

H	12.57304	4.72065	-3.51042
O	11.56081	6.41999	-1.74146
O	10.23053	2.19364	-2.86789
C	4.55224	-8.89805	-5.87111
C	4.32466	-8.22608	-7.07424
C	3.94581	-6.88292	-7.05838
C	4.40329	-8.23427	-4.65371
C	4.03236	-6.88857	-4.65673
C	3.79916	-6.20407	-5.84736
H	4.84159	-9.94451	-5.87719
H	4.44021	-8.74822	-8.01879
H	3.49801	-5.16310	-5.81267
H	3.76443	-6.35656	-7.99049
H	4.56700	-8.74695	-3.71168
O	3.79541	-6.21842	-3.45684
C	0.90785	-2.57606	-5.38343
C	1.69355	-2.78923	-4.25030
C	0.05690	-3.57810	-5.85422
C	1.62724	-4.02045	-3.59665
C	0.00421	-4.80514	-5.19009
C	0.79283	-5.03877	-4.06321
O	2.48808	-4.18976	-2.52238
H	0.96236	-1.61774	-5.89092
H	2.36021	-2.02207	-3.87196
H	-0.55788	-3.40643	-6.73214
H	-0.64633	-5.59448	-5.55441
H	0.77231	-5.99872	-3.56032
C	8.09702	-4.72162	6.25530
C	7.19540	-4.61075	5.19581

C	8.81137	-5.90434	6.45162
C	7.01382	-5.69691	4.34246
C	8.61646	-6.98422	5.58748
C	7.71206	-6.89059	4.53031
O	6.04579	-5.57082	3.35011
H	8.24363	-3.87807	6.92298
H	6.63293	-3.69973	5.02094
H	9.51528	-5.98567	7.27379
H	9.16410	-7.90925	5.73961
H	7.53919	-7.72744	3.86283
C	4.44454	-9.85528	6.34925
C	4.14315	-8.93989	7.35861
C	4.54276	-9.43392	5.02234
C	3.94709	-7.59434	7.03921
C	4.34288	-8.08858	4.72079
C	4.05148	-7.15782	5.71903
H	3.71927	-6.87654	7.82123
H	4.59779	-10.90279	6.59030
H	4.06209	-9.27181	8.38879
H	4.77097	-10.12837	4.22073
O	4.52974	-7.69832	3.39746
H	3.91828	-6.11323	5.46043
C	5.65543	-0.18339	-4.69426
C	5.63690	0.98944	-3.94027
C	5.38786	-1.41659	-4.09570
C	5.36476	0.91065	-2.57301
C	5.09990	-1.47678	-2.73037
C	5.09213	-0.31202	-1.96152
O	5.26549	2.04438	-1.77560

H	5.87250	-0.12919	-5.75673
H	5.82438	1.95327	-4.40005
H	5.40313	-2.32560	-4.68830
H	4.87770	-2.43118	-2.26382
H	4.87943	-0.33494	-0.89790
C	1.28105	2.48524	-5.65132
C	2.25957	3.22107	-4.98118
C	0.62556	1.43497	-5.00676
C	2.57658	2.89009	-3.66548
C	0.95908	1.11147	-3.68879
C	1.94113	1.83368	-3.01110
O	3.60536	3.60162	-3.05510
H	1.02660	2.74156	-6.67526
H	2.77789	4.04527	-5.45956
H	-0.14582	0.87357	-5.52471
H	0.45775	0.28943	-3.18737
H	2.21875	1.58667	-1.99246
C	6.54001	8.54689	4.41106
C	6.51729	9.58249	5.34637
C	6.10122	8.79502	3.11221
C	6.05401	10.84830	4.98487
C	5.64506	10.05774	2.73085
C	5.61893	11.08065	3.67810
H	6.89090	7.55375	4.67078
H	6.85662	9.39450	6.36049
H	5.32594	10.23006	1.70899
H	5.26396	12.06517	3.38923
C	10.09697	10.37489	1.79096
C	10.09521	11.60621	1.13158

C	9.19756	9.37432	1.42464
C	9.18756	11.83708	0.09693
C	8.30376	9.61824	0.38079
C	8.28807	10.84125	-0.28642
H	10.79587	10.19210	2.60145
H	10.79670	12.38107	1.42418
H	9.17767	8.42055	1.94004
O	7.33544	8.68591	0.02081
H	7.57691	10.99641	-1.09084
H	6.03240	11.65008	5.71612
H	9.18047	12.79179	-0.42019
O	6.21734	7.75655	2.19299
H	-1.47471	5.01758	2.02345

14. References

S1 Gaussian 09, Revision C.01, M. J. Frisch, G. W. Trucks, H. B. Schlegel, G. E. Scuseria, M. A. Robb, J. R. Cheeseman, G. Scalmani, V. Barone, B. Mennucci, G. A. Petersson, H. Nakatsuji, M. Caricato, X. Li, H. P. Hratchian, A. F. Izmaylov, J. Bloino, G. Zheng, J. L. Sonnenberg, M. Hada, M. Ehara, K. Toyota, R. Fukuda, J. Hasegawa, M. Ishida, T. Nakajima, Y. Honda, O. Kitao, H. Nakai, T. Vreven, J. A. Montgomery, Jr., J. E. Peralta, F. Ogliaro, M. Bearpark, J. J. Heyd, E. Brothers, K. N. Kudin, V. N. Staroverov, T. Keith, R. Kobayashi, J. Normand, K. Raghavachari, A. Rendell, J. C. Burant, S. S. Iyengar, J. Tomasi, M. Cossi, N. Rega, J. M. Millam, M. Klene, J. E. Knox, J. B. Cross, V. Bakken, C. Adamo, J. Jaramillo, R. Gomperts, R. E. Stratmann, O. Yazyev, A. J. Austin, R. Cammi, C. Pomelli, J. W. Ochterski, R. L. Martin, K. Morokuma, V. G. Zakrzewski, G. A. Voth, P. Salvador, J. J. Dannenberg, S. Dapprich, A. D. Daniels, O. Farkas, J. B. Foresman, J. V. Ortiz, J. Cioslowski, and D.J. Fox, Gaussian, Inc., Wallingford CT, 2010.

S2 N. F. Mott, R. W. Gurney, *Electronic processes in ionic crystals*. The Clarendon Press: New York, 1940.

S3 D. Pintossi, A. Colombo, M. Levi, C. Dragonetti, S. Turri and G. Griffini, *J. Mater. Chem. A*, 2017, **5**, 9067–9075.

S4 L. Yao, A. Rahmanudin, X. A. Jeanbourquin, X. Yu, M. Johnson, N. Guijarro, A. Sekar and K. Sivula, *Adv. Funct. Mater.*, 2018, **28**, 1–8.

S5 F. Javier Céspedes-Guirao, K. Ohkubo, S. Fukuzumi, Á. Sastre-Santos and F. Fernández-Lázaro, *J. Org. Chem.*, 2009, **74**, 5871–5880.

S6 J. Gorman, R. Pandya, J. R. Allardice, M. B. Price, T. W. Schmidt, R. H. Friend, A. Rao and N. J. L. K. Davis, *J. Phys. Chem. C*, 2019, **123**, 3433–3440.

S7 B. Ding, Y. Xiao, H. Zhou, X. Zhang, C. Qu, F. Xu, Z. Deng, Z. Cheng and X. Hong, *J. Med.*

Chem., 2019, **62**, 2049–2059.
S8 S. Guo, L. Ma, J. Zhao, B. Küçüköz, A. Karatay, M. Hayvali, H. G. Yaglioglu and A. Elmali, *Chem. Sci.*, 2014, **5**, 489–500.
S9 J. R. Lakowicz, *Principles of Fluorescence Spectroscopy*, Springer US, Boston, MA, 2006.
S10 V. Bandi, F. P. D'Souza, H. B. Gobeze and F. D'Souza, *Chem. Commun.*, 2016, **52**, 579–581.
S11 H. B. Gobeze, V. Bandi and F. D'Souza, *Phys. Chem. Chem. Phys.*, 2014, **16**, 18720-18728.
S12 S. Gangada, M. Chakali, H. Mandal, N. Duvva, R. Chitta, G. Lingamallu and P. R. Bangal, *Phys. Chem. Chem. Phys.*, 2018, **20**, 21352-21367.
S13 Y. Chen, L. Wan, X. Yu, W. Li, W. Bian and J. Jiang, *Org. Lett.*, 2011, **13**, 5774-5777.
S14 N. B. Khadke, A. A. Patil, D. Y. Patil and A. V. Borhade, *J. Fluor.*2019, **29**, 837–843.
S15 P. Thordarson, *Chem. Soc. Rev.* 2011, **40**, 1305–1323.
S16 A. Pomorski, T. Kochańczyk, A. Miłoch and A. Krężel, *Anal. Chem.* 2013, **85**, 11479−11486.
S17 A. M. Hessels and M. Merkx, *ACS Sensors* 2016, **1**, 498−502.
S18 K. Okamoto, H. Imahori and S. Fukuzumi, *J. Am. Chem. Soc.* 2003, **125**, 7014-7021.
S19 Y.V. Zatsikha, T. S. Blesener, P. C. Goff, A. T. Healy, R. K. Swedin, D. E. Herbert, G. T. Rohde, K. Chanawanno, C. J. Ziegler, R. V. Belosludov, D. A. Blank and V. N. Nemykin, *J. Phys, Chem. C*, 2018, **122**, 27893–27916.
S20 Y. V. Zatsikha, C. D. Holstrom, K. Chanawanno, A. J. Osinski, C. J. Ziegler and V. N. Nemykin, *Inorg. Chem.*, 2017, **56**, 991–1000.
S21 F. Würthner and A. Sautter, *Chem. Commun.*, 2000, **2**, 445–446.